Leveraging host metabolism for bisdemethoxycurcumin production in *Pseudomonas putida*

Matthew R. Incha[1,2,3], Mitchell G. Thompson[1,2,3], Jacquelyn M. Blake-Hedges[1,2,4], Yuzhong Liu[1,2], Allison N. Pearson[1,2], Matthias Schmidt[1,2], Jennifer W. Gin[1,2], Christopher J. Petzold[1,2], Adam M. Deutschbauer[3,5], Jay D. Keasling[1,2,6,7,8]

[1]Joint BioEnergy Institute, 5885 Hollis Street, Emeryville, CA 94608, USA.

[2]Biological Systems & Engineering Division, Lawrence Berkeley National Laboratory, Berkeley, CA 94720, USA.

[3]Department of Plant and Microbial Biology, University of California, Berkeley, CA 94720, USA

[4]Department of Chemistry, University of California, Berkeley, CA 94720, USA

[5]Environmental Genomics and Systems Biology Division, Lawrence Berkeley National Laboratory, Berkeley, California, USA

[6]Department of Chemical and Biomolecular Engineering, University of California, Berkeley, CA 94720, USA

[7]The Novo Nordisk Foundation Center for Biosustainability, Technical University of Denmark, Denmark

[8]Center for Synthetic Biochemistry, Institute for Synthetic Biology, Shenzhen Institutes for Advanced Technologies, Shenzhen, China

ABSTRACT

Pseudomonas putida is a saprophytic bacterium with robust metabolisms and strong solvent tolerance making it an attractive host for metabolic engineering and bioremediation. Due to its diverse carbon metabolisms, its genome encodes an array of proteins and enzymes that can be readily applied to produce valuable products. In this work we sought to identify design principles and bottlenecks in the production of type III polyketide synthase (T3PKS)-derived compounds in *P. putida*. T3PKS products are widely used as nutraceuticals and medicines and often require aromatic starter units, such as coumaroyl-CoA, which is also an intermediate in the native coumarate catabolic pathway of *P. putida*. Using a randomly barcoded transposon mutant (RB-TnSeq) library, we assayed gene functions for a large portion of aromatic catabolism, confirmed known pathways, and proposed new annotations for two aromatic transporters. The 1,3,6,8-tetrahydroxynapthalene synthase of *Streptomyces coelicolor* (RppA), a microbial T3PKS, was then used to rapidly assay growth conditions for increased T3PKS product accumulation. The feruloyl/coumaroyl CoA synthetase (Fcs) of *P. putida* was used to supply coumaroyl-CoA for the curcuminoid synthase (CUS) of *Oryza sativa*, a plant T3PKS. We identified that accumulation of coumaroyl-CoA in this pathway results in extended growth lag times in *P. putida*. Deletion of the second step in coumarate catabolism, the enoyl-CoA hydratase-lyase (Ech), resulted in increased production of the type III polyketide bisdemethoxycurcumin.

1 INTRODUCTION

Secondary metabolites of fungi, plants, and bacteria have long been used as medicines and supplements (Hewlings and Kalman, 2017). Compounds such as naringenin, raspberry ketone, resveratrol, and curcumin are widely used nutraceuticals and are biosynthesized through similar pathways (Heller and Hahlbrock, 1980; Katsuyama et al., 2008; Schanz et al., 1992;

54 Smith, 1996). Commercially, these chemicals are either extracted directly from plants or
55 produced synthetically, as in the case of raspberry ketone (Smith, 1996). Renewable microbial
56 production of these compounds will decrease reliance on agriculture and fossil fuel-derived
57 chemical synthesis. The biosynthesis of these compounds (naringenin, raspberry ketone,
58 resveratrol, and curcumin) relies on a class of enzymes called type III polyketide synthases
59 (T3PKSs). T3PKSs carry out iterative Claisen condensation reactions typically with coenzyme A
60 (CoA)-based starter and extender units (Yu et al., 2012). In the case of the 1,3,6,8-
61 tetrahydroxynapthalene synthase of *Streptomyces coelicolor* (RppA) the starter and extender
62 units are simply malonyl-CoA, while in many plant T3PKSs the starter unit is a
63 phenylpropanoyl-CoA thioester, usually derived from ferulate, coumarate, or cinnamate
64 (Izumikawa et al., 2003; Wakimoto et al., 2012).
65 Coumarate and ferulate are components of lignin found in lignocellulosic hydrolysate
66 (LH), which has been proposed for use as a renewable feedstock for biocatalysis (Jönsson et al.,
67 2013; Lawther and Sun, 1996). Characteristics such as high solvent tolerance and diverse carbon
68 metabolisms are essential for microbes to be used in LH valorization. However, these robust
69 traits are lacking in commonly used model organisms, such as *Escherichia coli*, hindering
70 progress toward making LH a viable feedstock (Mills et al., 2009). Rather than developing these
71 characteristics in a microorganism *de novo*, a clear alternative is to source a microbe with the
72 desirable traits already available to it. The saprophytic bacterium *Pseudomonas putida* has long
73 been studied for its ability to catabolize aromatic compounds and withstand solvents, making it
74 an attractive host for LH upcycling (Guarnieri et al., 2017; Linger et al., 2014; Nozaki et al.,
75 1963).

76 In this work we sought to leverage the native catabolism of *P. putida* KT2440 for use in
77 the biosynthesis of a plant T3PKS product from coumarate. RppA of *S. coelicolor* was first
78 expressed to determine production conditions conducive to T3PKS product accumulation. Using
79 a randomly barcoded transposon mutant (RB-TnSeq) library of *P. putida*, we assayed for genes
80 involved in the catabolism of coumarate and seven other related aromatic compounds. We then
81 found that accumulation of coumaroyl-CoA by the activity of Fcs was toxic to *P. putida*. The
82 native feruloyl/coumaroyl-CoA synthetase (Fcs) of *P. putida* was then used to produce the
83 coumaroyl-CoA starter unit to the curcuminoid synthase (CUS) of *Oryza sativa*. Finally, relying
84 on the native expression levels of *fcs* from the chromosome and plasmid-based expression of
85 *CUS* (Figure 1), production of bisdemethoxycurcumin (BDC) from coumarate was achieved.

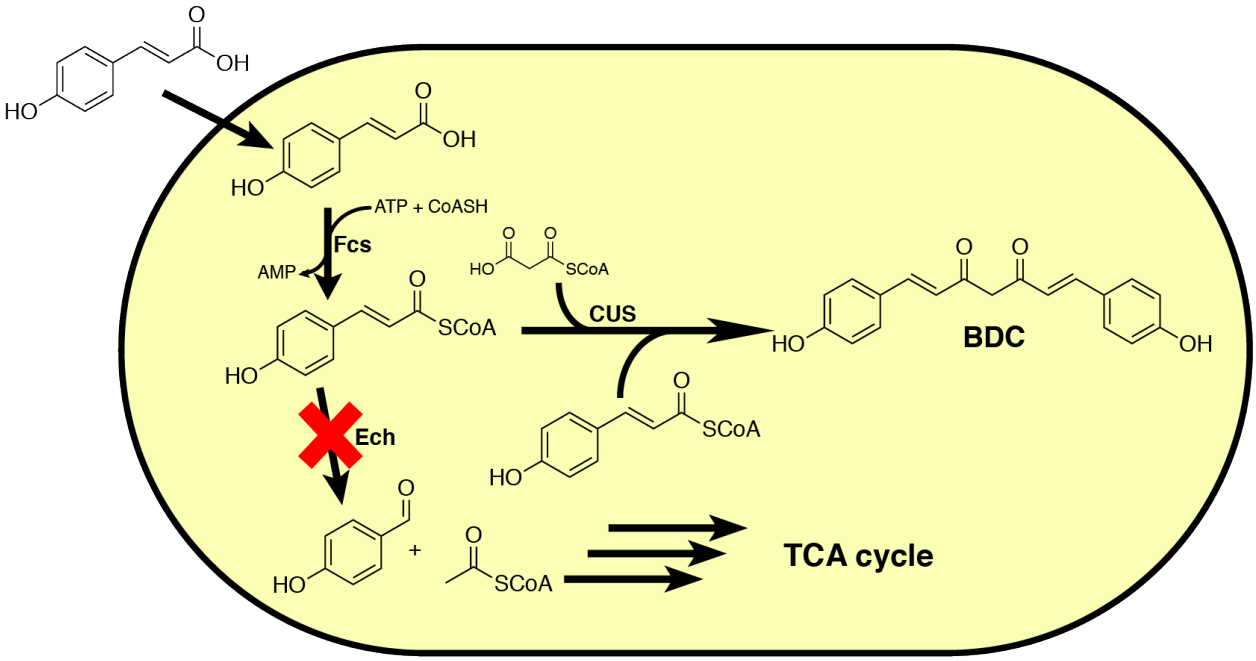

86

87 **Figure 1:** Diagram of the engineered *P. putida* strain used to produce bisdemethoxycurcumin.
88 Fcs is the feruloyl/coumaroyl-CoA synthetase native to *P. putida* KT2440. Ech is the native
89 enoyl-CoA hydratase-lyase which carries out the second step in coumarate catabolism and was
90 knocked out in our production host. CUS is the curcuminoid synthase from *O. sativa.* BDC is the
91 final curcuminoid product, bisdemethoxycurcumin.
92
93 **2 RESULTS**

94 2.1 RppA as a screen for optimal T3PKS production conditions

95 The tetrahydroxynaphthalene synthase of *Streptoyces coelicolor* was recently applied as a
96 biosensor for malonyl-CoA concentrations in several hosts including *P. putida* (Yang et al.,
97 2018). We sought to express this protein from the broad host range pBADT vector to assay
98 culture conditions for increased product accumulation in *P. putida*. RppA was initially codon
99 optimized for expression in *P. putida* and cloned into the construct pBADT-*rppA*-OW. We then
100 constructed two more plasmids, one with the complete *rppA* cloned from the *S. coelicolor*
101 genome (pBADT-*rppA*-NW) and another with a 3' truncation of 75 base pairs (pBADT-*rppA*-
102 NT) as this had been described previously to increase enzymatic activity (Izumikawa et al.,
103 2003).

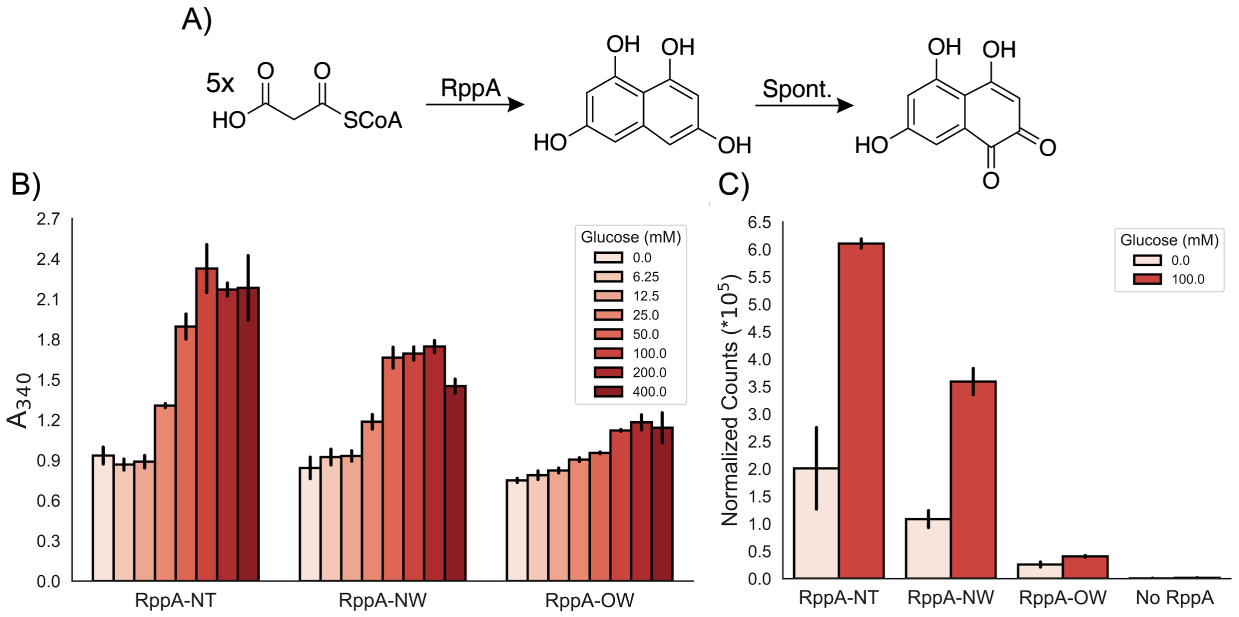

104 **Figure 2:** Flaviolin production as a reference for T3PKS activity. (A) Diagram of the pathway to
105 the red pigment, flaviolin, from RppA and subsequent spontaneous oxidation. (B) Absorbance
106 measurements at 340 nm of supernatants from cells expressing RppA variants in LB containing
107 different concentrations of glucose. Error bars indicate the standard deviation of three trials.
108 RppA-NW contains natural *S. coelicolor* codons, RppA-NT is the same as RppA-NW but with a
109 C-terminal truncation of 25 amino acids, and RppA-OW is translated from a transcript that was
110 codon optimized for *P. putida.* (C) RppA expression profile as determined by mass spectrometry
111 from lysates of cultures producing the RppA variants. The No RppA sample was extracted from

112 *P. putida* KT2440 carrying pBADT-RFP. Error bars indicate the standard deviation of three
113 replicates.
114
115
116 Since the product of RppA, 1,3,6,8-tetrahydroxynaphthalene, spontaneously oxidizes to
117 the red pigment flaviolin, we used a colorimetric assay to determine how glucose concentrations
118 affect the production of T3PKS products (Figure 2A). Concentrations of glucose ranging from 0
119 - 400 mM supplemented into LB medium were tested, and the production of flaviolin was
120 measured by absorbance at 340 nm, as previously reported (Yang et al., 2018). Unexpectedly,
121 the *rppA* expression vectors using the native *S. coelicolor* codons produced more flaviolin than
122 the *P. putida* codon optimized variant (Figure 2B). In all three constructs tested, there was an
123 increase in the accumulation of flaviolin in cultures containing greater than 25 mM glucose and
124 accumulation of flaviolin appeared to plateau at ~100 mM glucose (Figures 2B and S4). To
125 validate the observed red compound was flaviolin, we extracted, purified, and obtained an ^{1}H-
126 NMR spectrum for the red product using established methods (Figure S5A and S5B) (Gross et
127 al., 2006; Soga, 1982). The final yield from 100 mL of culture was ~6.5 mg.
128 Following this result, we sought to identify if increased protein abundance was the cause
129 for increased flaviolin production. When RppA was quantified using LC-MS, we observed an
130 increase in its relative abundance for all variants when 100 mM glucose was supplemented to the
131 medium. The abundance of RppA also was highest in the strains expressing the native genomic
132 sequence of *rppA* (Figure 2C).

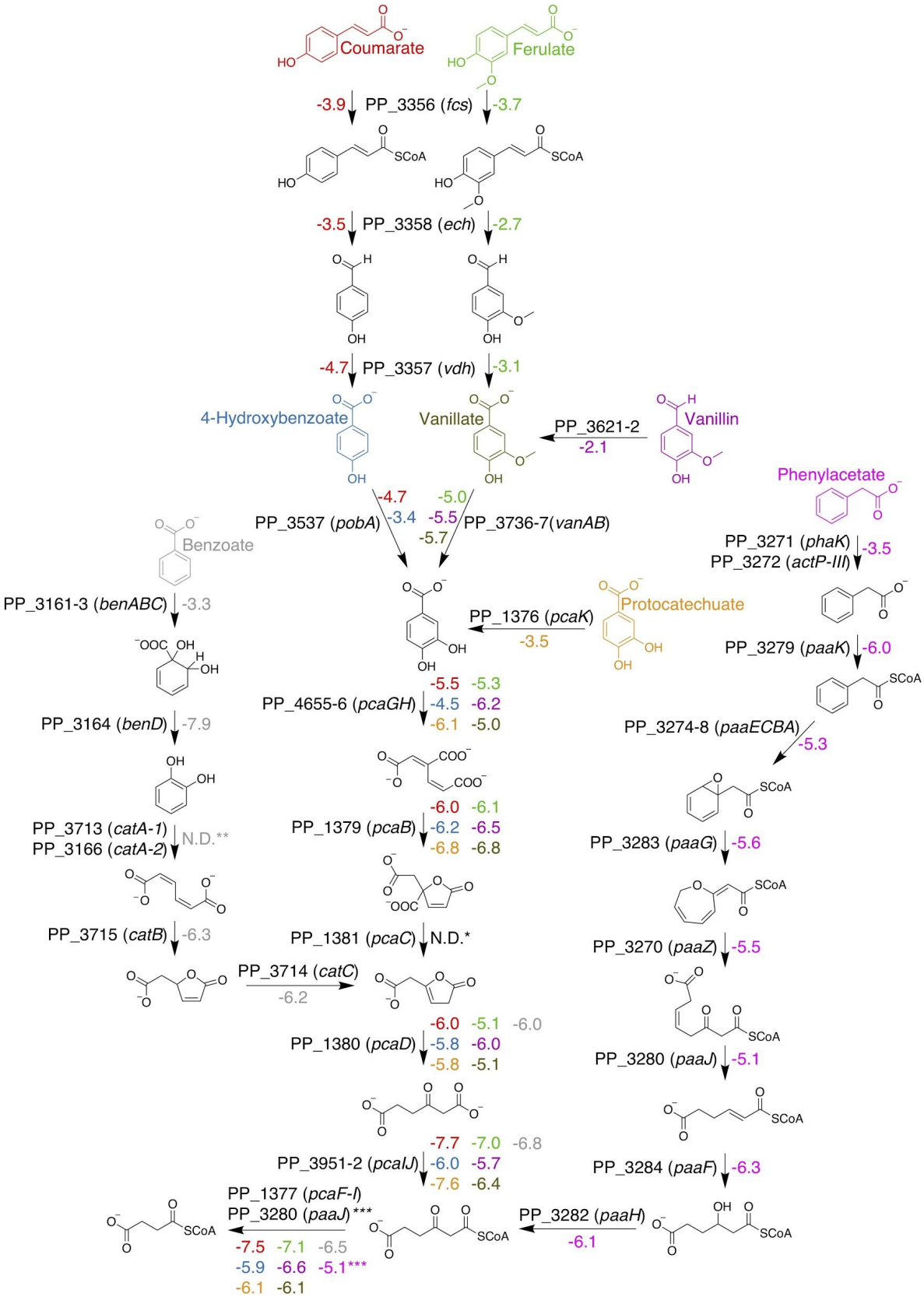
Coumarate
Ferulate
-3.9
PP_3356 (fcs)
-3.7
-3.5
PP_3358 (ech)
-2.7
-4.7
PP_3357 (vdh)
-3.1
4-Hydroxybenzoate
Vanillate
PP_3621-2
-2.1
Vanillin
Phenylacetate
-4.7
-3.4
-5.0
-5.5
-5.7
PP_3537 (pobA)
PP_3736-7(vanAB)
PP_3271 (phaK)
PP_3272 (actP-III)
-3.5
Benzoate
PP_3161-3 (benABC)
-3.3
PP_1376 (pcaK)
-3.5
Protocatechuate
PP_3279 (paaK)
-6.0
-5.5 -5.3
PP_4655-6 (pcaGH)
-4.5 -6.2
-6.1 -5.0
PP_3164 (benD)
-7.9
PP_3274-8 (paaECBA)
-5.3
-6.0 -6.1
PP_3713 (catA-1)
PP_3166 (catA-2)
N.D.**
PP_1379 (pcaB)
-6.2 -6.5
-6.8 -6.8
PP_3283 (paaG)
-5.6
PP_3715 (catB)
-6.3
PP_1381 (pcaC)
N.D.*
PP_3270 (paaZ)
-5.5
PP_3714 (catC)
-6.2
-6.0 -5.1 -6.0
PP_1380 (pcaD)
-5.8 -6.0
-5.8 -5.1
PP_3280 (paaJ)
-5.1
-7.7 -7.0 -6.8
PP_3951-2 (pcaIJ)
-6.0 -5.7
-7.6 -6.4
PP_3284 (paaF)
-6.3
PP_1377 (pcaF-I)
PP_3280 (paaJ)***
PP_3282 (paaH)
-6.1
-7.5 -7.1 -6.5
-5.9 -6.6 -5.1***
-6.1 -6.1

133

134 **Figure 3:** Overview of aromatic catabolism in *P. putida* KT2440. The colored and labelled
135 compounds depicted were fed as sole carbon sources to the barcoded transposon library. Fitness
136 values for each gene are the average of 2 replicate RB-TnSeq assays, and are colored
137 corresponding to the carbon source (gray: benzoate, red: coumarate, blue: 4-hydroxybenzoate,
138 light green: ferulate, dark green: vanillate, purple: vanillin, yellow: protocatechuate, pink:
139 phenylacetate). For reactions where multiple genes are necessary, i.e. enzyme complexes, the
140 fitness values for each gene involved in the reaction were averaged. *The t-score for *pcaC* was
141 insignificant ($|t_{score}| < 4.0$) and was excluded from our analysis. **Fitness values for these genes
142 were mild (fitness > -2.0) and excluded. ***Fitness value corresponds to *paaJ*.
143
144 <u>2.2 Functional genomics to validate aromatic catabolisms of *P. putida*</u>

145 While aromatic catabolism has been extensively studied in *P. putida*, essential genes
146 implicated in these pathways have been described as recently as 2019 (Price et al., 2019). The
147 genes involved in the first steps of coumarate catabolism reside in an operon with a putative
148 acyl-CoA dehydrogenase (*PP_3354*) and a putative beta-ketothiolase (*PP_3355*), which have
149 been proposed to be involved in an alternative catabolic pathway (Overhage et al., 1999). As
150 functional redundancy in coumarate catabolism could result in loss of the type III polyketide
151 precursor, coumaroyl-CoA, we sought to identify any pathways that could potentially impact
152 product titers. To assay for genes involved in coumarate and related aromatic metabolisms, we
153 grew a randomly barcoded transposon mutant (RB-TnSeq) library of *P. putida* KT2440 in
154 minimal medium with a variety of different aromatic compounds often found in LH (p-
155 coumarate, ferulate, benzoate, p-hydroxybenzoate, protocatechuate, vanillin, vanillate,
156 phenylacetate) and glucose as sole carbon sources. The fitness of each gene was calculated by
157 comparing the abundance of barcodes before versus after growth selection, using barcode
158 sequencing (BarSeq) (Rand et al., 2017; Wetmore et al., 2015). Negative values indicate that the
159 gene was important for growth in that condition.

160 The results of the RB-TnSeq assay validated that the primary route for ferulate and
161 coumarate catabolism is through the feruloyl/coumaroyl-CoA synthetase (Fcs) and the enoyl-
162 CoA hydratase lyase (Ech) (Figure 3 and Figure S1). The genes in the proposed secondary

163 pathway of coumarate and ferulate catabolism, *PP_3354* and *PP_3355*, had no significant fitness
164 phenotype, indicating that these genes are likely not necessary for coumarate or ferulate
165 catabolism (Plaggenborg et al., 2003).

166 Of all the known reactions depicted in the map of aromatic catabolism (Figure 3), we
167 observed significant negative fitness values for all but three of their corresponding genes: *catA-1*,
168 *catA-2*, and *pcaC*. Even though the fitness score was higher than our cutoff at -1.4, *catA-1* had a
169 significant |t-score| of 6.2 when grown on benzoate. This reflects previous work demonstrating
170 CatA-I is the preferred catechol 1,2-dioxygenase, while CatA-II acts as a "safety valve" to
171 handle high intracellular concentrations of catechol. It was also demonstrated that both catA-I
172 and catA-II need to be deleted to abolish growth on benzoate, and this likely explains why the
173 fitness value for catA-I was above our cut-off (Jiménez et al., 2014). In the case of *pcaC*, we
174 noticed that there was a strong phenotype (fitness < -2.0), but the significance fell below our
175 cutoff in all conditions tested ($|t_{score}| < 4.0$). This is likely due to the low frequency of transposon
176 insertions into this gene in the library (n=4).

177 While our results heavily support the current models of aromatic metabolism in *P. putida*,
178 our data also indicated that some gene annotations should be revised. *PP_3272* is currently
179 annotated as encoding an acetate permease (Kanehisa, 2019; Kanehisa et al., 2019; Kanehisa and
180 Goto, 2000). We observed that *PP_3272* had a significant phenotype when grown on
181 phenylacetate (Figure 3). Given these data and previously described homology to other systems
182 (Jiménez et al., 2002), *PP_3272* should be reannotated as the phenylacetate transporter (phaJ).
183 The *PP_1376* gene is annotated as encoding a 4-hydroxybenzoate transporter (Kanehisa, 2019;
184 Kanehisa et al., 2019; Kanehisa and Goto, 2000); however, we only observed a fitness detriment

185 for this gene with protocatechuate as the sole carbon source (Figure 3). Because of this, *PP_1376*
186 should be reannotated as a protocatechuate transporter.

187 2.3 Accumulation of coumaroyl-CoA is toxic to *P. putida*

188 The first step in the biosynthetic pathway for bisdemethoxycurcumin is the activation of
189 coumarate with coenzyme A (CoASH) (Figure 1). Because *Pseudomonas putida* KT2440
190 natively produces coumaroyl-CoA during coumarate catabolism, we knocked out the subsequent
191 gene in the native catabolic pathway, *ech*, to prevent *P. putida* from consuming this necessary
192 precursor (Figure 1) (Jiménez et al., 2002). Initial production experiments in Δ*ech* strains
193 overexpressing *fcs* and *CUS* from a synthetic operon resulted in an extended lag phase (data not
194 shown). To determine the cause, we overexpressed *fcs* alone under control of the arabinose-
195 inducible *araBAD* promoter (P_{BAD}) in the presence and absence of coumarate. Increasing the
196 inducer concentration resulted in increased lag times only when coumarate was present in the
197 medium (Figures 4A and S6). This suggested that the coumaroyl-CoA intermediate is toxic to *P.*
198 *putida*.

199 To determine if coumaroyl-CoA concentrations are elevated in cultures expressing *fcs*,
200 cultures carrying pBADT-*fcs* were induced with L-arabinose. After a 7-hour growth period, 5
201 mM coumarate was supplemented to the medium. Following supplementation, growth was
202 stunted and remained relatively constant over the course of 11 hours. The concentration of
203 coumaroyl-CoA was highest in samples one hour after coumarate was supplemented into the
204 medium; this was observed regardless of the *ech* genotype (Figure 4B). We therefore sought to
205 minimize the burden of this intermediate by relying on the native chromosomal expression of *fcs*
206 in future experiments.

207

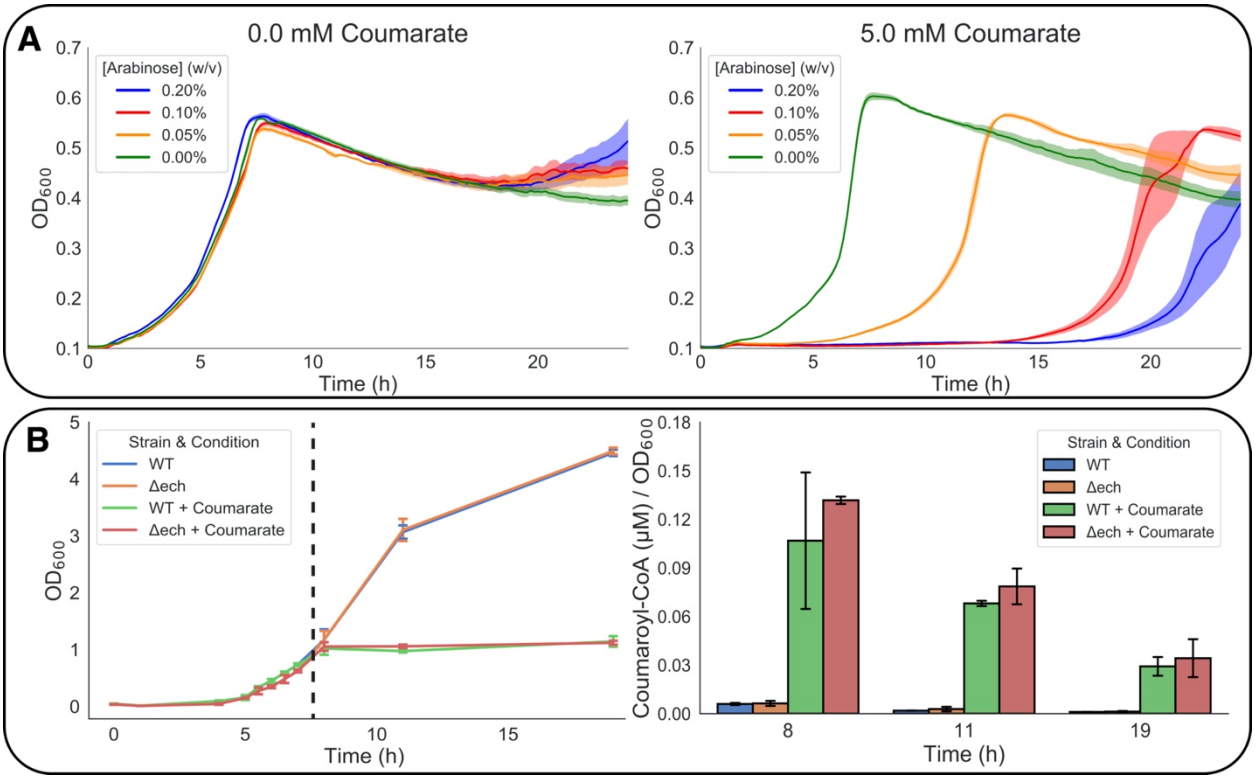

208 **Figure 4:** Production of coumaroyl-CoA inhibits growth of *P. putida.* (A) 24 hour growth
209 curves of KT2440 Δ*ech* carrying pBADT-*fcs* in LB induced with varying concentrations of
210 arabinose and no added coumarate (left), or 5 mM coumarate (right). Error bars are +/- the
211 standard deviation of three replicates. (B) Growth curve (left) and normalized abundance of
212 coumaroyl-CoA (right) in KT2440 (WT) and KT2440 Δ*ech* (Δ*ech*). Cultures expressing *fcs* were
213 supplemented with 0 or 5 mM coumarate at hour 7 (marked with dashed line). Coumaroyl-CoA
214 concentrations were normalized by OD_{600}. Error bars are +/- the standard deviation of three
215 replicates.
216
217 <u>2.4 Production of bisdemethoxycurcumin</u>

218 In order to produce bisdemethoxycurcumin in *P. putida*, we constructed the biochemical
219 pathway outlined in Figure 1. Exogenously added coumarate is activated by the native
220 feruloyl/coumaroyl-CoA synthetase of *P. putida* (Fcs), then two resultant coumaroyl-CoA
221 molecules are condensed with malonyl-CoA by the curcuminoid synthase of *O. sativa* (CUS) to
222 yield bisdemethoxycurcumin (Katsuyama et al., 2007b). The CoA synthetase, *fcs*, was expressed
223 from its native chromosomal locus, while *CUS* was expressed from the pBADT plasmid and
224 induced with L-arabinose (Bi et al., 2013).

225 Our initial production strategy was to induce *CUS* until the cultures reached stationary
226 phase. Then the cultures were pelleted and resuspended in fresh LB medium supplemented with
227 5 mM coumarate. These samples were then incubated for another 72 hours. A similar approach
228 had been used successfully in *E. coli* (Katsuyama et al., 2007a); however, our titers were less
229 than 0.5 mg/L (Figure S2). Given that bisdemethoxycurcumin is insoluble in water (Javeri and
230 Chand, 2016), a 10 % v/v oleyl alcohol overlay was used to extract the product as the
231 fermentation progressed. Production levels were low (approximately 0.1 mg/L) in *P. putida* Δ*ech*
232 when the medium was supplemented with 10 mM coumarate, likely due to the toxicity of
233 coumaroyl-CoA (Figure 5). Supplementation with 5 mM coumarate resulted in a ~5-fold
234 increase in bisdemethoxycurcumin titers in the *P. putida* Δ*ech* strain relative to wild-type (Figure
235 5).

236
237
238
239
240
241
242
243
244
245
246
247
248
249
250

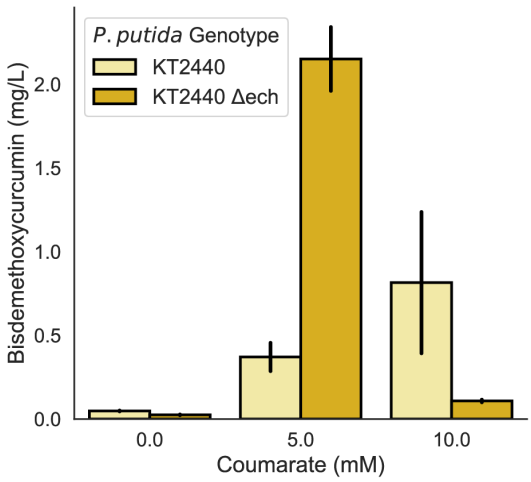

251
252 **Figure 5**: Bisdemethoxycurcumin titers in *P. putida* KT2440 Δ*ech* and in wildtype KT2440
253 harboring pBADT-CUS. *CUS* was induced with 2 % w/v L-arabinose. Error bars are +/- the
254 standard deviation of three biological replicates.
255
256 **3. DISCUSSION**

257 *Pseudomonas putida* is among the most well studied saprophytic bacteria. Its diverse
258 metabolisms enable it to catabolize a wide variety of complex carbon sources, including

259 lignocellulosic hydrolysate (Wang et al., 2019). The robust catabolic pathways of *P. putida*,
260 while useful for producing valuable molecules from diverse carbon sources, can also serve as an
261 obstacle to achieving high product titers as it can often metabolize the desired products (Mitchell
262 G Thompson et al., 2019). Given recent advances in gene editing techniques (Aparicio et al.,
263 2019, 2018; Cook et al., 2018; Martínez-García and de Lorenzo, 2011; Wirth et al., 2019) and
264 our ability to rapidly assay for gene function with transposon site sequencing (Price et al., 2018;
265 Rand et al., 2017; Wetmore et al., 2015), engineering non-model hosts like *P. putida* for
266 industrial applications has become less challenging.

267 Using RB-TnSeq mutant fitness assays we were able to rapidly confirm entire pathways
268 of aromatic catabolism (Figure 3 and S1). The genes downstream of *fcs*, *PP_3354* and *PP_3355*
269 previously described as a possible alternative route for coumarate/ferulate catabolism (Jiménez et
270 al., 2002; Overhage et al., 1999; Priefert et al., 2001), showed no significant fitness detriment on
271 any of the carbon sources tested. These genes may be structural remnants of a β-oxidation
272 pathway that eventually evolved into the coumarate/ferulate pathway requiring *fcs*, *ech*, and *vdh*
273 (Jiménez et al., 2002; Overhage et al., 1999; Priefert et al., 2001). We then proposed revised
274 annotations of two genes required for transport of the aromatic compounds, phenylacetate
275 (*PP_3272*) and protocatechuate (*PP_1376*), an important plant hormone and lignin metabolite
276 respectively (Wightman and Lighty, 1982). There is a large amount of information in these data
277 encompassing regulatory and structural genetic elements that could be useful to engineers and
278 biologists.

279 Heterologous expression of bacterial T3PKSs, including the tetrahydroxynapthalene
280 synthase of *S. coelicolor* (RppA), has previously been demonstrated in *P. putida* KT2440 (Gross
281 et al., 2006; Yang et al., 2018). Using variants of *rppA*, we were able to rapidly screen type III

282 polyketide production conditions. Expressing the codon optimized variant we created in this
283 study, *rppA*-OW, resulted in less flaviolin production and less protein production than the native
284 codon variants *rppA*-NW and *rppA*-NT. It is possible that there are some factors affecting
285 heterologous protein expression that are not sufficiently accounted for in current codon
286 optimization algorithms (Cambray et al., 2018). However, we demonstrated in all our constructs
287 that increasing the glucose concentration had a considerable effect on the production of flaviolin
288 (Figure 2 and S4).

289 Higher flaviolin accumulation with increased glucose concentrations could be due to
290 increased flux to malonyl-CoA, a known limiting reactant to the biosynthesis of plant T3PKS
291 products (Katsuyama et al., 2008; Zang et al., 2019), or due to increased functional protein
292 expression. As the relative abundance of RppA increased when the culture was grown in the
293 presence of 100 mM glucose, we hypothesize this likely contributed to the increased flaviolin
294 titer observed in this condition (Figure 2B and 2C). The exact cause for the increase in protein
295 abundance requires more detailed investigation. These T3PKS "sensors" have broad utility in
296 both rapidly assaying culture conditions, as described here, and as high-throughput screens of
297 genetic libraries for increased malonyl-CoA accumulation (Yang et al., 2018). Future work
298 could employ these sensors to screen for increased intracellular malonyl-CoA concentrations
299 from a complex growth medium like LH.

300 To provide the coumaroyl-CoA substrate for the bisdemethoxycurucumin T3PKS, CUS,
301 we sought to use the native CoA synthetase (Fcs) of *P. putida*. Plasmid-based induction of *fcs*
302 expression in the presence of coumarate, however, resulted in an increase in lag times due to the
303 build-up of the toxic coumaroyl-CoA intermediate (Figures 4A, 4B, and S6). Neither the
304 accumulation of coumaroyl-CoA nor the resultant growth inhibition seemed to be significantly

305 affected by the genetic presence of *ech* (Figure 4B). The reduction in intracellular coumaroyl-
306 CoA concentrations following the addition of coumarate was also not dependent on the presence
307 of *ech* (Figure 4B). This reduction in thioester concentrations may be the result of nonspecific
308 thioesterase activity, or spontaneous hydrolysis of coumaroyl-CoA.

309 The toxicity of hydroxycinnamate thioesters has been reported in *Acinetobacter baylyi*
310 following disruptions in the gene encoding its enoyl-CoA hydratase lyase, and it was observed in
311 *E. coli* expressing the *A. baylyi fcs* homolog in the presence of coumarate (Parke and Ornston,
312 2004). This toxicity could have been limiting other systems using bacterial coumaroyl-CoA
313 synthetases, but the defective growth phenotype may not have been observed due to differences
314 in experimental design (Park et al., 2009; Santos et al., 2011). The exact cause for coumaroyl-
315 CoA toxicity remains unclear and will be the subject of future investigations.

316 To engineer *P. putida* for bisdemethoxycurcumin production, we deleted the native
317 enoyl-CoA hydratase lyase (*ech*) responsible for the conversion of coumaroyl-CoA to acetyl-
318 CoA and p-hydroxybenzaldehyde. In order to relieve some of the observed coumaroyl-CoA
319 toxicity, we relied on the native genomic copy of *fcs* instead of a plasmid-based system. We
320 demonstrated that native expression of *fcs* generates sufficient coumaroyl-CoA for curcuminoid
321 synthase (CUS). Extraction of the product during growth using an oleyl alcohol overlay also
322 significantly enhanced titers (Figure S2 and 5). In the final *P. putida* production strain, we
323 achieved production of bisdemethoxycurcumin at titers of 2.15 mg/L (Figure 5).

324 This work is a significant first step towards the production of plant T3PKS-derived
325 compounds in *P. putida*, but several issues remain to be addressed. In particular, our final
326 bisdemthoxycurcumin titer of 2.15 mg/L is far lower than the 91.3 mg/l titer first described in *E.*
327 *coli* (Katsuyama et al., 2008). Several methods have been proposed to enhance the production of

328 curcuminoids and similar T3PKS derived compounds in microbial hosts. In one such approach,
329 the metabolic burden of product, protein, and plasmid DNA synthesis was spread across several
330 microbial strains in a synthetic co-culture (Fang et al., 2018). Since phenylpropanoid
331 overproducing strains of *P. putida* have been described (Nijkamp et al., 2007, 2005), a co-culture
332 method could be explored for the biosynthesis of plant T3PKS products in this host. It is also
333 quite clear that more extensive pathway balancing will be required to mitigate the intermediate
334 toxicity we have observed. As we continue to understand more about the metabolism of *P.*
335 *putida* and learn to engineer it more effectively, this host will become an increasingly attractive
336 chassis for renewable chemical biosynthesis.
337

338 **4. METHODS**

339 4.1 Media, chemicals, and culture conditions

340 General *E. coli* cultures were grown in Luria-Bertani (LB) Miller medium (BD
341 Biosciences, USA) at 37 °C, while *P. putida* was grown at 30 °C. MOPS minimal medium was
342 used where indicated and comprised of the following: 32.5 μM $CaCl_2$, 0.29 mM K_2SO_4, 1.32 mM
343 K_2HPO_4, 8 μM $FeCl_2$, 40 mM MOPS, 4 mM tricine, 0.01 mM $FeSO_4$, 9.52 mM NH_4Cl, 0.52 mM
344 $MgCl_2$, 50 mM NaCl, 0.03 μM $(NH_4)_6Mo_7O_{24}$, 4 μM H_3BO_3, 0.3 μM $CoCl_2$, 0.1 μM $CuSO_4$,
345 0.8 μM $MnCl_2$, and 0.1 μM $ZnSO_4$ (LaBauve and Wargo, 2012). Cultures were supplemented
346 with kanamycin (50 mg/L, Sigma Aldrich, USA) when indicated. Technical grade oleyl alcohol
347 was acquired from Alfa Aesar (Alfa Aesar, Thermo Fisher Scientific). Coenzyme A (lithium
348 salt) was purchased from CoALA Biosciences (CoALA Biosciences, USA). All other
349 compounds were purchased through Sigma Aldrich (Sigma Aldrich, USA). Construction of *P.*
350 *putida* deletion mutants was performed as described previously (Thompson et al., 2019).

351 4.2 Strains and plasmids

352 Bacterial strains and plasmids used in this work are listed in Table 1. All strains and
353 plasmids created in this work are available through the public instance of the JBEI registry
354 https://public-registry.jbei.org. All plasmids were designed using Device Editor and Vector
355 Editor software, while all primers used for the construction of plasmids were designed using j5
356 software (Chen et al., 2012; Ham et al., 2012; Hillson et al., 2012). Plasmids were assembled via
357 Gibson Assembly using standard protocols (Gibson et al., 2009), or Golden Gate Assembly using
358 standard protocols (Engler et al., 2008). Plasmids were routinely isolated using the Qiaprep Spin
359 Miniprep kit (Qiagen, USA), and all primers were purchased from Integrated DNA Technologies
360 (IDT, Coralville, IA).

361 **Table 1: Strains and plasmids used in this study**

Strain	**JBEI Part ID**	**Reference**
E. coli DH10B		(Grant et al., 1990)
E. coli BL21(DE3)		Novagen
P. putida KT2440		ATCC 47054
P. putida KT2440 Δ*ech*		
Plasmids		
pET28		Novagen
pBADT		(Bi et al., 2013)
pBADT-*CUS*	JBx_134311	This work
pBADT-*rppA*-NT	JBx_134312	This work
pBADT-*rppA*-NW	JBx_134313	This work
pBADT-*rppA*-OW	JBx_134314	This work

pBADT-*fcs*	JBx_134315	This work
pBADT-*fcs*-*CUS*	JBx_134316	This work
pMQ30		(Shanks et al., 2009)
pMQ30-*PP_3358*		(Park et al., 2019)

362

363 4.3 Plate based growth assays

364 Growth studies of bacterial strains were conducted using microplate reader kinetic assays.
365 Overnight cultures were inoculated into 10 mL of LB medium from single colonies, and grown
366 at 30 °C. These cultures were then diluted 1:100 into 500 µL of LB medium with appropriate
367 concentrations of arabinose and p-coumarate in 48-well plates (Falcon, 353072). Plates were
368 sealed with a gas-permeable microplate adhesive film (VWR, USA), and optical density and
369 fluorescence were monitored for 48 hours in a Biotek Synergy 4 plate reader (BioTek, USA) at
370 30 °C with fast continuous shaking. Optical density was measured at 600 nm. The amount of
371 time necessary for the culture to reach an OD_{600} of 0.16 was defined as the lag time.

372 4.4 HPLC detection of bisdemethoxycurcumin

373 HPLC analysis was performed on an Agilent Technologies 1200 series liquid
374 chromatography instrument coupled to a Diode Array Detector (Agilent Technologies, USA).
375 Compounds were separated at a constant flow rate of 0.4 mL/min over a Kinetex C18 column
376 (2.6 µm diameter, 100Å particle size, dimensions 100 x 3.00 mm, Phenomenex, USA) held at 50
377 °C. The mobile phase consisted of H_2O + 0.1% trifluoroacetic acid (A) and acetonitrile + 0.1%
378 trifluoroacetic acid (B). Separation was performed using the following gradient method: 0-3
379 minutes 95% A, 3-15 minutes 95-5% A, 15-17 minutes 5% A, 17-17.5 minutes 5-95% A, 17.5-
380 20 minutes 95% A. The presence of bisdemethoxycurcumin was monitored and quantified at 440
381 nm.

382 4.5 RB-TnSeq experiments and analysis

383 BarSeq-based experiments utilized the *P. putida* RB-TnSeq library, JBEI-1, which has
384 been described previously (Thompson et al., 2019). An aliquot of JBEI-1 was thawed on ice,
385 diluted into 25 mL of LB medium supplemented with kanamycin and grown to an OD_{600} of 0.5 at
386 30 °C. Three 1 mL aliquots of the library were pelleted and stored at -80 °C to later serve as the
387 t_0 of gene abundance. Libraries were then washed in MOPS minimal medium and diluted 1:50 in
388 MOPS minimal medium with 10 mM p-coumarate, ferulate, benzoate, p-hydroxybenzoate,
389 protocatechuate, vanillin, vanillate, phenylacetate, or D-glucose. Cells were grown in 600 µL of
390 medium in 96-well deep well plates (VWR). Plates were sealed with a gas-permeable microplate
391 adhesive film (VWR, USA), and then grown at 30 °C in an INFORS HT Multitron (Infors USA
392 Inc.), with shaking at 700 rpm. Two 600-µL samples were combined, pelleted, and stored at -
393 80 °C until analysis by BarSeq, which was performed as previously described (Rand et al., 2017;
394 Wetmore et al., 2015). All fitness data are publicly available at http://fit.genomics.lbl.gov.

395 4.5 Curcuminoid production

396 For production of bisdemthoxycurcumin without an overlay, an overnight culture of *P.*
397 *putida* KT2440 Δ*ech* + pBADT-CUS was diluted 1:100 into 5 mL of LB supplemented with 50
398 mg/L kanamycin, 1 % w/v L-arabinose, and 100 mM glucose. The culture was grown to
399 stationary phase over 12 hours then pelleted in a centrifuge at 5000 xg for 5 minutes. The cell
400 pellets were resuspended in 2 mL of fresh LB with 50 mg/L kanamycin, 0.5 % L-arabinose, 100
401 mM glucose, and 5 mM coumarate. The culture was allowed to proceed for 72 hours.

402 For experiments employing an overlay, overnights of *P. putida* harboring pBADT-CUS
403 were diluted 1:100 into 25 mL of fresh LB supplemented with 50 mg/L kanamycin, and 100 mM
404 glucose. Arabinose and coumarate were added at the beginning of the fermentation at

405 concentrations indicated. A 2.5 mL overlay of oleyl alcohol was added to extract the
406 bisdemethoxycurcumin during growth. The fermentation was allowed to proceed for 72 hours.

407 4.6 Curcuminoid extraction

408 For cultures lacking an overlay, 0.5 mL of culture was acidified to pH 3 with 3 N HCl.
409 Bisdemethoxycurcumin was then extracted with an equal volume of ethyl acetate. 250 µL of the
410 ethyl acetate layer was removed and the solvent was allowed to evaporate overnight. The dried
411 samples were then resuspended in 50 µL of acetonitrile for analysis with HPLC-DAD.

412 For cultures with an overlay, the cultures were acidified to pH 3 with 3 N HCl. Acidified
413 cultures were then pelleted in a centrifuge and the oleyl alcohol overlays were removed. To
414 quantify bisdemethoxycurcumin, 100 µL of the extracted overlays were added to a black, clear
415 bottom 96-well plate and absorbance was measured at 425 nm in a Biotek Synergy 4 plate reader
416 (BioTek, USA). A standard curve was made with bisdemethoxycurcumin standards dissolved in
417 oleyl alcohol (Figure S3)

418 4.7 Flaviolin production and targeted proteomic analysis

419 Colonies of *P. putida* KT2440 strains carrying pBADT-*rppA*-NW, pBADT-*rppA*-NT,
420 and pBADT-*rppA*-OW were used to inoculate LB or MOPS minimal medium with 50 mg/L
421 kanamycin and cultured overnight. The overnight culture was then diluted 1/100 into fresh
422 medium with 0.2 % w/v L-arabinose, 50 mg/L kanamycin, and 400, 200, 100, 50, 25, 12.5, 6.25
423 or 0 mM glucose. Cultures were conducted in 24-well deep-well plates and allowed to proceed
424 for 48 hours. Cultures were then pelleted in a centrifuge at 5000 xg for 5 minutes. Supernatants
425 were removed, aliquoted into a 96-well black clear bottom plate, and the absorbance was
426 measured at 340 nm in a Biotek Synergy 4 plate reader (BioTek, USA). For cultures expressing
427 *rppA* variants in LB, the supernatants were too opaque with red product and needed to be diluted

428 1:5 in fresh LB for accurate absorbance measurements. Supernatants of strains cultured in
429 minimal medium were not diluted before absorbance measurements.
430 Samples for intracellular targeted proteomic analysis were grown for 48 hours in 5 mL
431 LB supplemented with 0 mM or 100 mM glucose. Then, 2 mL of the culture were then pelleted
432 by centrifugation, the supernatant was decanted, and the pellets were stored at -80 °C. Proteins
433 were extracted and analyzed using a variation of a previously-described workflow (Chen et al.,
434 2019).
435 4.8 Flaviolin purification
436 An overnight culture of *P. putida* KT2440 carrying pBADT-rppA-NT was diluted 1:100
437 into 100 mL of LB supplemented with 25 mg/L kanamycin, 0.2% *w*/*v* *L*-arabinose, and 100 mM
438 glucose. The culture was shaken for 48 hours at 30 °C in a 500 mL baffled Erlenmeyer flask.
439 Following fermentation, the red supernatant was removed, acidified with 10 mL 10 *N* HCl, and
440 extracted twice with equal volumes of ethyl acetate. The combined organic phase was evaporated
441 leaving a black solid, which was then dissolved in ethyl acetate and methanol (7:3). The extract
442 components were then separated using preparative thin layer chromatography (TLC, silica gel).
443 The red band was isolated from the TLC plate, extracted with methanol, and filtered. The
444 methanol was evaporated *in vacuo* leaving dark red solid with a yield of ~6.5 mg. The identity of
445 the flaviolin was then validated with ^{1}H-NMR. ^{1}H-NMR (400 MHz, CD_3OD) δ 6.99 (s, 1 H),
446 6.47 (s, 1 H), 5.58 (s, 1 H) (Figure S5A and S5B).
447 4.9 Synthesis of coumaroyl-CoA standard

Scheme 1

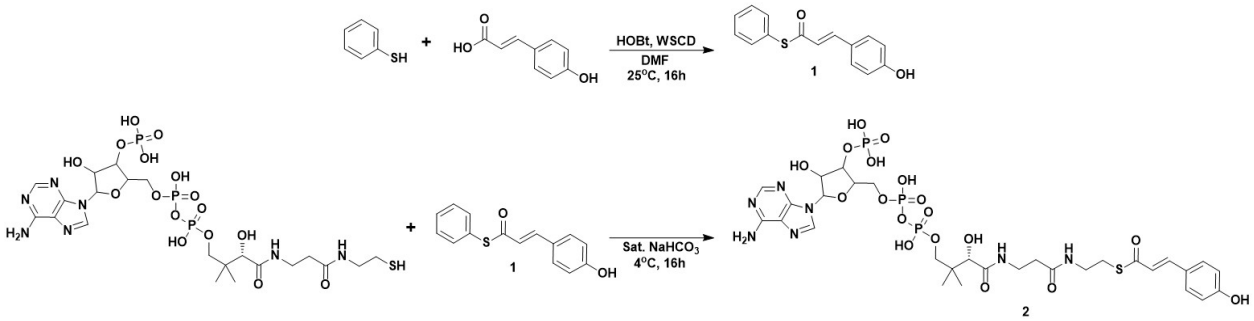

Coumaroyl-Coenzyme A (**2**) was synthesized in two steps according to Scheme 1. *S*-phenyl (*E*)-3-(4-hydroxyphenyl)prop-2-enethioate (**1**) was synthesized according to previous literature (Hori et al., 2012). 1-(3-Dimethylaminopropyl)-3-ethylcarbodiimide hydrochloride (WSCD·HCl, 1.48 g, 7.3 mmol), 1-hydroxybenzotriazole (HOBt, 1.12 g, 7.3 mmol), and 4-hydroxycinnamic acid (1 g, 6.1 mmol) were dissolved in DMF (100 mL) and stirred for 1 h at room temperature. Thiophenol (0.610 mL, 6.1 mmol) was subsequently added to the mixture and stirred overnight at room temperature. After the solvent was removed *in vacuo*, water and dichloromethane (DCM) were added to the mixture. The organic layers were combined, dried over Na_2SO_4, and evaporated. The product was purified with silica-gel column chromatography and eluted with DCM to yield *S*-phenyl (*E*)-3-(4-hydroxyphenyl)prop-2-enethioate as a white solid (**1**, 468 mg, 30%).

To synthesize coumaroyl-CoA (**2**), coenzyme A lithium salt (7.7 mg, 10 μmol) was dissolved in a solution of saturated sodium bicarbonate (750 μL) which had been pre-chilled to 4 °C. *S*-phenyl (*E*)-3-(4-hydroxyphenyl)prop-2-enethioate (30 mg, 117 μmol) was added to the solution. The solution was mixed for 16 hours at 4 °C then quenched via the addition of 6M HCl to bring the pH of the solution to ~2. The mixture was extracted with ethyl acetate (2 x 2 mL), then coumaroyl-CoA was purified from the remaining aqueous phase via preparatory HPLC.

Coumaroyl-CoA was purified using an Agilent 1260 series preparatory HPLC system equipped with a 900 μL sample loop and a UV detector coupled to a fraction collector.

468 Compounds were separated over an Agilent Zorbax SB-C18 preparatory column (9.4 x 50 mm, 5
469 µm particle size) using a mobile phase composed of 10 mM ammonium formate, pH 4.5 (solvent
470 A) and methanol (solvent B) using the following method:
471

Time (min)	**%A**	**%B**	**Flow rate (mL/min)**
0	95	5	10
1	95	5	10
8	5	95	10
10	5	95	10
11	95	5	10
16	95	5	10

472

473 The fraction collector was programmed to collect peaks absorbing at a wavelength of 260
474 nm and that eluted between 3.6 and 4.6 minutes. The fractions containing coumaroyl-CoA were
475 identified by direct infusion onto an Applied Biosystems 4000 QTRAP mass spectrometer
476 system operating with the following parameters: Q1 MS mode, scan range 100-1000 m/z,
477 declustering potential: 70, entrance potential: 10, curtain gas: 10, IonSpray Voltage: 4800,
478 Temperature: 300, Ion Source Gases: 40. Fractions containing coumaroyl-CoA were combined
479 and lyophilized, yielding coumaroyl-CoA as a white powder (6 mg,

480 4.10 LC-MS/MS analysis of intracellular Coenzyme A esters

481 *P. putida* KT2440 and *P. putida* Δ*ech* cells carrying pBADT-*fcs* were cultured overnight.
482 Cultures were inoculated 1:100 into 25 mL LB supplemented with 100 mM glucose and 0.2%
483 w/v L-arabinose. Cells were cultured at 30 °C for 7 hours then coumarate was added to a final

484 concentration of 5 mM. 10 mL of culture were taken at hours 8, 11, and 19 and pelleted in a
485 centrifuge. Cell pellets were resuspended in 1 mL ice cold methanol and stored at -80 °C until
486 workup.

487 Coenzyme A esters were extracted as follows: to the 1 mL methanol resuspensions, 0.5
488 mL of ice cold LC grade water and 0.25 mL ice cold LC chloroform. Samples were vortexed to
489 mix after each addition. Samples were then centrifuged at maximum speed for 2 minutes to
490 promote phase separation, after which 0.5 mL of the top aqueous phase was removed and
491 transferred to an Amicon 3 kDa molecular weight cutoff centrifuge filter (Sigma Aldrich, USA).
492 Extracts were filtered by spinning in a benchtop centrifuge at 4 °C for 90 minutes at 13000g. The
493 flow through was lyophilized for 24 hours to concentrate the sample. Lyophilized fractions were
494 resuspended in 0.1 mL of ice cold 60:40 (v/v) LC grade acetonitrile: LC grade water, and 35 µL
495 of the aqueous layer was removed for LC-MS/MS analysis.

496 CoA extracts were analyzed using an Applied Biosystems 4000 QTRAP mass
497 spectrometer coupled to an Aglient 1100-1200 series HPLC. Compounds were separated over a
498 Phenomenex Kinetex XB-C18 column (100 x 3 mm, 100 Å, 2.6 µm particle size) held at 50 °C.
499 The mobile phase was composed of 10 mM ammonium formate, pH 4.5 (solvent A) and
500 acetonitrile (solvent B) the following LC method was used:

Time (min)	**%A**	**%B**	**Flow rate (µL/min)**
0	98	2	400
2	98	2	400
5.5	2	98	400
8.5	2	98	400
9.5	98	2	400
12.75	98	2	400

The mass spectrometer was operated in positive ion mode using the following parameters: Curtain gas: 20 L/min, Collision gas: medium, Ionspray voltage: 4500 V, Temperature: 250 °C, Ion source gas 1: 20 L/min, Ion source gas 2: 10 L/min, Declustering potential: 0, Entrance potential: 10, Collision cell exit potential: 10. Coumaroyl-CoA was detected in multiple reaction monitoring (MRM) mode by monitoring the following transition: 914.16 m/z → 407.16 m/z using a collision energy of 47.8 V. Data was imported into Skyline targeted mass spectrometry environment (v. 3.7.0 11317) and peaks were integrated using Skyline's embedded integration function. Coumaroyl-CoA was quantified relative to a standard curve that was generated by calculating the linear regression of 3 individual injections of each concentration within the standard curve (R^2= 0.9982).

Acknowledgements

We would like to thank Professor Mattheos Koffas for providing us with the plasmid pEMT6-4CL-CUS. We thank Jesus Barajas for his careful reading of this manuscript and helpful suggestions during preparation. We also thank Morgan Price for assistance in analyzing RB-TnSeq data.

This work was part of the DOE Joint BioEnergy Institute (https://www.jbei.org) supported by the U. S. Department of Energy, Office of Science, Office of Biological and Environmental Research, supported by the U.S. Department of Energy, Energy Efficiency and Renewable Energy, Bioenergy Technologies Office, through contract DE-AC02-05CH11231 between Lawrence Berkeley National Laboratory and the U.S. Department of Energy. The views and opinions of the authors expressed herein do not necessarily state or reflect those of the

United States Government or any agency thereof. Neither the United States Government nor any agency thereof, nor any of their employees, makes any warranty, expressed or implied, or assumes any legal liability or responsibility for the accuracy, completeness, or usefulness of any information, apparatus, product, or process disclosed, or represents that its use would not infringe privately owned rights. The United States Government retains and the publisher, by accepting the article for publication, acknowledges that the United States Government retains a nonexclusive, paid-up, irrevocable, worldwide license to publish or reproduce the published form of this manuscript, or allow others to do so, for United States Government purposes. The Department of Energy will provide public access to these results of federally sponsored research in accordance with the DOE Public Access Plan (http://energy.gov/downloads/doe-public-access-plan)

Contributions

Conceptualization, M.R.I., M.G.T., J.M.B; Methodology, M.R.I., M.G.T., J.M.B.,Y.L.,C.J.P.; Investigation, M.R.I., M.G.T., J.M.B., Y.L., M.S., A.N.P., J.W.G.; Writing – Original Draft, M.R.I.; Writing – Review and Editing, All authors.; Resources and supervision, C.J.P, A.M.D., J.D.K.

Competing Interests

J.D.K. has financial interests in Amyris, Lygos, Demetrix, Napigen and Maple Bio

Supplementary Figures

546 **Figure S1:** Heatmap of RB-TnSeq mutant fitness data. Genes shown have fitness defects ($-\log_2$

547 < -2) and with statistical significance ($|t_{score}| > 4$) in at least one tested condition which show no

548 significant fitness defects when grown on glucose.

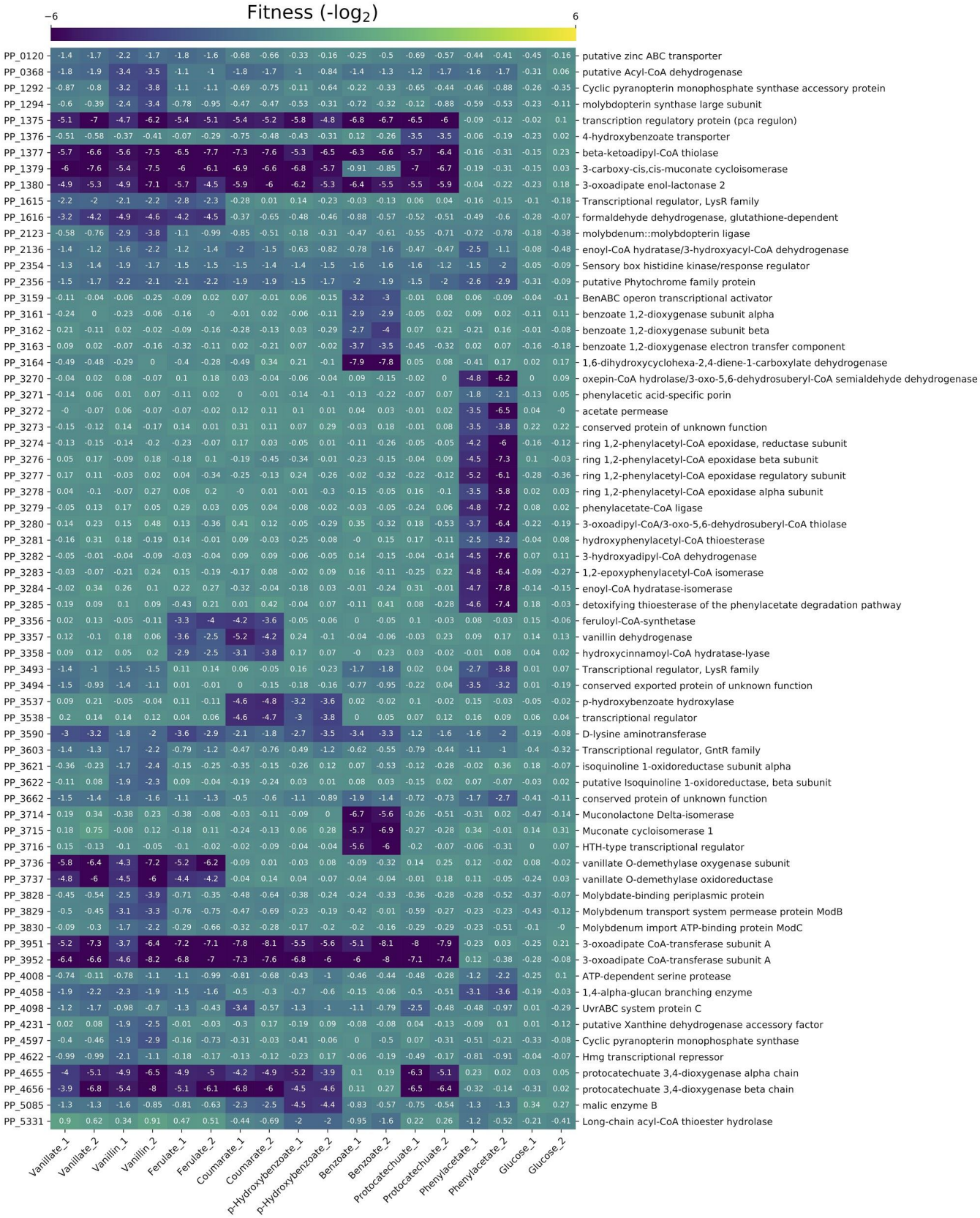
Fitness (-log2)
−6
6
Vanillate_1 Vanillate_2 Vanillin_1 Vanillin_2 Ferulate_1 Ferulate_2 Coumarate_1 Coumarate_2 p-Hydroxybenzoate_1 p-Hydroxybenzoate_2 Benzoate_1 Benzoate_2 Protocatechuate_1 Protocatechuate_2 Phenylacetate_1 Phenylacetate_2 Glucose_1 Glucose_2
PP_0120 -1.4 -1.7 -2.2 -1.7 -1.8 -1.6 -0.68 -0.66 -0.33 -0.16 -0.25 -0.5 -0.69 -0.57 -0.44 -0.41 -0.45 -0.16 putative zinc ABC transporter
PP_0368 -1.8 -1.9 -3.4 -3.5 -1.1 -1 -1.8 -1.7 -1 -0.84 -1.4 -1.3 -1.2 -1.7 -1.6 -1.7 -0.31 0.06 putative Acyl-CoA dehydrogenase
PP_1292 -0.87 -0.8 -3.2 -3.8 -1.1 -1.1 -0.69 -0.75 -0.11 -0.64 -0.22 -0.33 -0.65 -0.44 -0.46 -0.88 -0.26 -0.35 Cyclic pyranopterin monophosphate synthase accessory protein
PP_1294 -0.6 -0.39 -2.4 -3.4 -0.78 -0.95 -0.47 -0.47 -0.53 -0.31 -0.72 -0.32 -0.12 -0.88 -0.59 -0.53 -0.23 -0.11 molybdopterin synthase large subunit
PP_1375 -5.1 -7 -4.7 -6.2 -5.4 -5.1 -5.4 -5.2 -5.8 -4.8 -6.8 -6.7 -6.5 -6 -0.09 -0.12 -0.02 0.1 transcription regulatory protein (pca regulon)
PP_1376 -0.51 -0.58 -0.37 -0.41 -0.07 -0.29 -0.75 -0.48 -0.43 -0.31 0.12 -0.26 -3.5 -3.5 -0.06 -0.19 -0.23 0.02 4-hydroxybenzoate transporter
PP_1377 -5.7 -6.6 -5.6 -7.5 -6.5 -7.7 -7.3 -7.6 -5.3 -6.5 -6.3 -6.6 -5.7 -6.4 -0.16 -0.31 -0.15 0.23 beta-ketoadipyl-CoA thiolase
PP_1379 -6 -7.6 -5.4 -7.5 -6 -6.1 -6.9 -6.6 -6.8 -5.7 -0.91 -0.85 -7 -6.7 -0.19 -0.31 -0.15 0.03 3-carboxy-cis,cis-muconate cycloisomerase
PP_1380 -4.9 -5.3 -4.9 -7.1 -5.7 -4.5 -5.9 -6 -6.2 -5.3 -6.4 -5.5 -5.5 -5.9 -0.04 -0.22 -0.23 0.18 3-oxoadipate enol-lactonase 2
PP_1615 -2.2 -2 -2.1 -2.2 -2.8 -2.3 -0.28 0.01 0.14 -0.23 -0.03 -0.13 0.06 0.04 -0.16 -0.15 -0.1 -0.18 Transcriptional regulator, LysR family
PP_1616 -3.2 -4.2 -4.9 -4.6 -4.2 -4.5 -0.37 -0.65 -0.48 -0.46 -0.88 -0.57 -0.52 -0.51 -0.49 -0.6 -0.28 -0.07 formaldehyde dehydrogenase, glutathione-dependent
PP_2123 -0.58 -0.76 -2.9 -3.8 -1.1 -0.99 -0.85 -0.51 -0.18 -0.31 -0.47 -0.61 -0.55 -0.71 -0.72 -0.78 -0.18 -0.38 molybdenum::molybdopterin ligase
PP_2136 -1.4 -1.2 -1.6 -2.2 -1.2 -1.4 -2 -1.5 -0.63 -0.82 -0.78 -1.6 -0.47 -0.47 -2.5 -1.1 -0.08 -0.48 enoyl-CoA hydratase/3-hydroxyacyl-CoA dehydrogenase
PP_2354 -1.3 -1.4 -1.9 -1.7 -1.5 -1.5 -1.5 -1.4 -1.4 -1.5 -1.6 -1.6 -1.6 -1.2 -1.5 -2 -0.05 -0.09 Sensory box histidine kinase/response regulator
PP_2356 -1.5 -1.7 -2.2 -2.1 -2.1 -2.2 -1.9 -1.9 -1.5 -1.7 -2 -1.9 -1.5 -2 -2.6 -2.9 -0.31 -0.09 putative Phytochrome family protein
PP_3159 -0.11 -0.04 -0.06 -0.25 -0.09 0.02 0.07 -0.01 0.06 -0.15 -3.2 -3 -0.01 0.08 0.06 -0.09 -0.04 -0.1 BenABC operon transcriptional activator
PP_3161 -0.24 0 -0.23 -0.06 -0.16 -0 -0.01 0.02 -0.06 -0.11 -2.9 -2.9 -0.05 0.02 0.09 0.02 -0.11 0.11 benzoate 1,2-dioxygenase subunit alpha
PP_3162 0.21 -0.11 0.02 -0.02 -0.09 -0.16 -0.28 -0.13 0.03 -0.29 -2.7 -4 0.07 0.21 -0.21 0.16 -0.01 -0.08 benzoate 1,2-dioxygenase subunit beta
PP_3163 0.09 0.02 -0.07 -0.16 -0.32 -0.11 0.02 -0.21 0.07 -0.02 -3.7 -3.5 -0.45 -0.32 0.02 0.07 -0.16 -0.18 benzoate 1,2-dioxygenase electron transfer component
PP_3164 -0.49 -0.48 -0.29 0 -0.4 -0.28 -0.49 0.34 0.21 -0.1 -7.9 -7.8 0.05 0.08 -0.41 0.17 0.02 0.17 1,6-dihydroxycyclohexa-2,4-diene-1-carboxylate dehydrogenase
PP_3270 -0.04 0.02 0.08 -0.07 0.1 0.18 0.03 -0.04 -0.06 -0.04 0.09 -0.15 -0.02 0 -4.8 -6.2 0 0.09 oxepin-CoA hydrolase/3-oxo-5,6-dehydrosuberyl-CoA semialdehyde dehydrogenase
PP_3271 -0.14 0.06 0.01 0.07 -0.11 0.02 0 -0.01 -0.14 -0.1 -0.13 -0.22 -0.07 0.07 -1.8 -2.1 -0.13 0.05 phenylacetic acid-specific porin
PP_3272 -0 -0.07 0.06 -0.07 -0.07 -0.02 0.12 0.11 0.1 0.01 0.04 0.03 -0.01 0.02 -3.5 -6.5 0.04 -0 acetate permease
PP_3273 -0.15 -0.12 0.14 -0.17 0.14 0.01 0.31 0.11 0.07 0.29 -0.03 0.18 -0.01 0.08 -3.5 -3.8 0.22 0.22 conserved protein of unknown function
PP_3274 -0.13 -0.15 -0.14 -0.2 -0.23 -0.07 0.17 0.03 -0.05 0.01 -0.11 -0.26 -0.05 -0.05 -4.2 -6 -0.16 -0.12 ring 1,2-phenylacetyl-CoA epoxidase, reductase subunit
PP_3276 0.05 0.17 -0.09 0.18 -0.18 0.1 -0.19 -0.45 -0.34 -0.01 -0.23 -0.15 -0.04 0.09 -4.5 -7.3 0.1 -0.03 ring 1,2-phenylacetyl-CoA epoxidase beta subunit
PP_3277 0.17 0.11 -0.03 0.02 0.04 -0.34 -0.25 -0.13 0.24 -0.26 -0.02 -0.32 -0.22 -0.12 -5.2 -6.1 -0.28 -0.36 ring 1,2-phenylacetyl-CoA epoxidase regulatory subunit
PP_3278 0.04 -0.1 -0.07 0.27 0.06 0.2 -0 0.01 -0.01 -0.3 -0.15 -0.05 0.16 -0.1 -3.5 -5.8 0.02 0.03 ring 1,2-phenylacetyl-CoA epoxidase alpha subunit
PP_3279 -0.05 0.13 0.17 0.05 0.29 0.03 0.05 0.04 -0.08 -0.02 -0.03 -0.05 -0.24 0.06 -4.8 -7.2 0.08 0.02 phenylacetate-CoA ligase
PP_3280 0.14 0.23 0.15 0.48 0.13 -0.36 0.41 0.12 -0.05 -0.29 0.35 -0.32 0.18 -0.53 -3.7 -6.4 -0.22 -0.19 3-oxoadipyl-CoA/3-oxo-5,6-dehydrosuberyl-CoA thiolase
PP_3281 -0.16 0.31 0.18 -0.19 0.14 -0.01 0.09 -0.03 -0.25 -0.08 -0 0.15 0.17 -0.11 -2.5 -3.2 -0.04 0.08 hydroxyphenylacetyl-CoA thioesterase
PP_3282 -0.05 -0.01 -0.04 -0.09 -0.03 -0.04 0.09 0.09 -0.06 -0.05 0.14 -0.15 -0.04 -0.14 -4.5 -7.6 0.07 0.11 3-hydroxyadipyl-CoA dehydrogenase
PP_3283 -0.03 -0.07 -0.21 0.24 0.15 -0.19 -0.17 0.08 -0.02 0.09 0.16 -0.11 -0.25 0.22 -4.8 -6.4 -0.09 -0.27 1,2-epoxyphenylacetyl-CoA isomerase
PP_3284 -0.02 0.34 0.26 0.1 0.22 0.27 -0.32 -0.04 -0.18 0.03 -0.01 -0.24 0.31 -0.01 -4.7 -7.8 -0.14 -0.15 enoyl-CoA hydratase-isomerase
PP_3285 0.19 0.09 0.1 0.09 -0.43 0.21 0.01 0.42 -0.04 0.07 -0.11 0.41 0.08 -0.28 -4.6 -7.4 0.18 -0.03 detoxifying thioesterase of the phenylacetate degradation pathway
PP_3356 0.02 0.13 -0.05 -0.11 -3.3 -4 -4.2 -3.6 -0.05 -0.06 0 -0.05 0.1 -0.03 0.08 -0.03 0.15 -0.06 feruloyl-CoA-synthetase
PP_3357 0.12 -0.1 0.18 0.06 -3.6 -2.5 -5.2 -4.2 0.24 -0.1 -0.04 -0.06 -0.03 0.23 0.09 0.17 0.14 0.13 vanillin dehydrogenase
PP_3358 0.09 0.12 0.05 0.2 -2.9 -2.5 -3.1 -3.8 0.17 0.07 -0 0.23 0.03 -0.02 -0.01 0.08 0.04 0.02 hydroxycinnamoyl-CoA hydratase-lyase
PP_3493 -1.4 -1 -1.5 -1.5 0.11 0.14 0.06 -0.05 0.16 -0.23 -1.7 -1.8 0.02 0.04 -2.7 -3.8 0.01 0.07 Transcriptional regulator, LysR family
PP_3494 -1.5 -0.93 -1.4 -1.1 0.01 -0.01 0 -0.15 -0.18 -0.16 -0.77 -0.95 -0.22 0.04 -3.5 -3.2 0.01 -0.19 conserved exported protein of unknown function
PP_3537 0.09 0.21 -0.05 -0.04 0.11 -0.11 -4.6 -4.8 -3.2 -3.6 0.02 -0.02 0.1 -0.02 0.15 -0.03 -0.05 -0.02 p-hydroxybenzoate hydroxylase
PP_3538 0.2 0.14 0.14 0.12 0.04 0.06 -4.6 -4.7 -3 -3.8 0 0.05 0.07 0.12 0.16 0.09 0.06 0.04 transcriptional regulator
PP_3590 -3 -3.2 -1.8 -2 -3.6 -2.9 -2.1 -1.8 -2.7 -3.5 -3.4 -3.3 -1.2 -1.6 -1.6 -2 -0.19 -0.08 D-lysine aminotransferase
PP_3603 -1.4 -1.3 -1.7 -2.2 -0.79 -1.2 -0.47 -0.76 -0.49 -1.2 -0.62 -0.55 -0.79 -0.44 -1.1 -1 -0.4 -0.32 Transcriptional regulator, GntR family
PP_3621 -0.36 -0.23 -1.7 -2.4 -0.15 -0.25 -0.35 -0.15 -0.26 0.12 0.07 -0.53 -0.12 -0.28 -0.02 0.36 0.18 -0.07 isoquinoline 1-oxidoreductase subunit alpha
PP_3622 -0.11 0.08 -1.9 -2.3 0.09 -0.04 -0.19 -0.24 0.03 0.01 0.08 0.03 -0.15 0.02 0.07 -0.07 -0.03 0.02 putative Isoquinoline 1-oxidoreductase, beta subunit
PP_3662 -1.5 -1.4 -1.8 -1.6 -1.1 -1.3 -0.5 -0.6 -1.1 -0.89 -1.9 -1.4 -0.72 -0.73 -1.7 -2.7 -0.41 -0.11 conserved protein of unknown function
PP_3714 0.19 0.34 -0.38 0.23 -0.38 -0.08 -0.03 -0.11 -0.09 0 -6.7 -5.6 -0.26 -0.51 -0.31 0.02 -0.47 -0.14 Muconolactone Delta-isomerase
PP_3715 0.18 0.75 -0.08 0.12 -0.18 0.11 -0.24 -0.13 0.06 0.28 -5.7 -6.9 -0.27 -0.28 0.34 -0.01 0.14 0.31 Muconate cycloisomerase 1
PP_3716 0.15 -0.13 -0.1 -0.05 -0.1 -0.02 -0.02 -0.09 -0.04 -0.04 -5.6 -6 -0.2 -0.07 -0.06 -0.31 0 0.07 HTH-type transcriptional regulator
PP_3736 -5.8 -6.4 -4.3 -7.2 -5.2 -6.2 -0.09 0.01 -0.03 0.08 -0.09 -0.32 0.14 0.25 0.12 -0.02 0.08 -0.02 vanillate O-demethylase oxygenase subunit
PP_3737 -4.8 -6 -4.5 -6 -4.4 -4.2 -0.04 0.14 0.04 -0.07 -0.04 -0.04 -0.01 0.18 0.11 -0.05 -0.24 0.03 vanillate O-demethylase oxidoreductase
PP_3828 -0.45 -0.54 -2.5 -3.9 -0.71 -0.35 -0.48 -0.64 -0.38 -0.24 -0.24 -0.33 -0.36 -0.28 -0.28 -0.52 -0.37 -0.07 Molybdate-binding periplasmic protein
PP_3829 -0.5 -0.45 -3.1 -3.3 -0.76 -0.75 -0.47 -0.69 -0.23 -0.19 -0.42 -0.01 -0.59 -0.27 -0.23 -0.23 -0.43 -0.12 Molybdenum transport system permease protein ModB
PP_3830 -0.09 -0.3 -1.7 -2.2 -0.29 -0.66 -0.32 -0.28 -0.17 -0.2 -0.2 -0.16 -0.29 -0.29 -0.23 -0.51 -0.1 -0 Molybdenum import ATP-binding protein ModC
PP_3951 -5.2 -7.3 -3.7 -6.4 -7.2 -7.1 -7.8 -8.1 -5.5 -5.6 -5.1 -8.1 -8 -7.9 -0.23 0.03 -0.25 0.21 3-oxoadipate CoA-transferase subunit A
PP_3952 -6.4 -6.6 -4.6 -8.2 -6.8 -7 -7.3 -7.6 -6.8 -6 -6 -8 -7.1 -7.4 0.12 -0.38 -0.28 -0.08 3-oxoadipate CoA-transferase subunit A
PP_4008 -0.74 -0.11 -0.78 -1.1 -1.1 -0.99 -0.81 -0.68 -0.43 -1 -0.46 -0.44 -0.48 -0.28 -1.2 -2.2 -0.25 0.1 ATP-dependent serine protease
PP_4058 -1.9 -2.2 -2.3 -1.9 -1.5 -1.6 -0.5 -0.3 -0.7 -0.6 -0.15 -0.06 -0.5 -0.51 -3.1 -3.6 -0.19 -0.03 1,4-alpha-glucan branching enzyme
PP_4098 -1.2 -1.7 -0.98 -0.7 -1.3 -0.43 -3.4 -0.57 -1.3 -1 -1.1 -0.79 -2.5 -0.48 -0.48 -0.97 0.01 -0.29 UvrABC system protein C
PP_4231 0.02 0.08 -1.9 -2.5 -0.01 -0.03 -0.3 0.17 -0.19 0.09 -0.08 -0.08 0.04 -0.13 -0.09 0.1 0.01 -0.12 putative Xanthine dehydrogenase accessory factor
PP_4597 -0.4 -0.46 -1.9 -2.9 -0.16 -0.73 -0.31 -0.03 -0.41 -0.06 0 -0.5 0.07 -0.31 -0.51 -0.21 -0.33 -0.08 Cyclic pyranopterin monophosphate synthase
PP_4622 -0.99 -0.99 -2.1 -1.1 -0.18 -0.17 -0.13 -0.12 -0.23 0.17 -0.06 -0.19 -0.49 -0.17 -0.81 -0.91 -0.04 -0.07 Hmg transcriptional repressor
PP_4655 -4 -5.1 -4.9 -6.5 -4.9 -5 -4.2 -4.9 -5.2 -3.9 0.1 0.19 -6.3 -5.1 0.23 0.02 0.03 0.05 protocatechuate 3,4-dioxygenase alpha chain
PP_4656 -3.9 -6.8 -5.4 -8 -5.1 -6.1 -6.8 -6 -4.5 -4.6 0.11 0.27 -6.5 -6.4 -0.32 -0.14 -0.31 0.02 protocatechuate 3,4-dioxygenase beta chain
PP_5085 -1.3 -1.3 -1.6 -0.85 -0.81 -0.63 -2.3 -2.5 -4.5 -4.4 -0.83 -0.57 -0.75 -0.54 -1.3 -1.3 0.34 0.27 malic enzyme B
PP_5331 0.9 0.62 0.34 0.91 0.47 0.51 -0.44 -0.69 -2 -2 -0.95 -1.6 0.22 0.26 -1.2 -0.52 -0.21 -0.41 Long-chain acyl-CoA thioester hydrolase

Figure S2: HPLC trace of curcumin extracted from *P. putida* KT2440 Δ*ech* + pBADT-CUS overlaid with a 3.125 mg/L standard

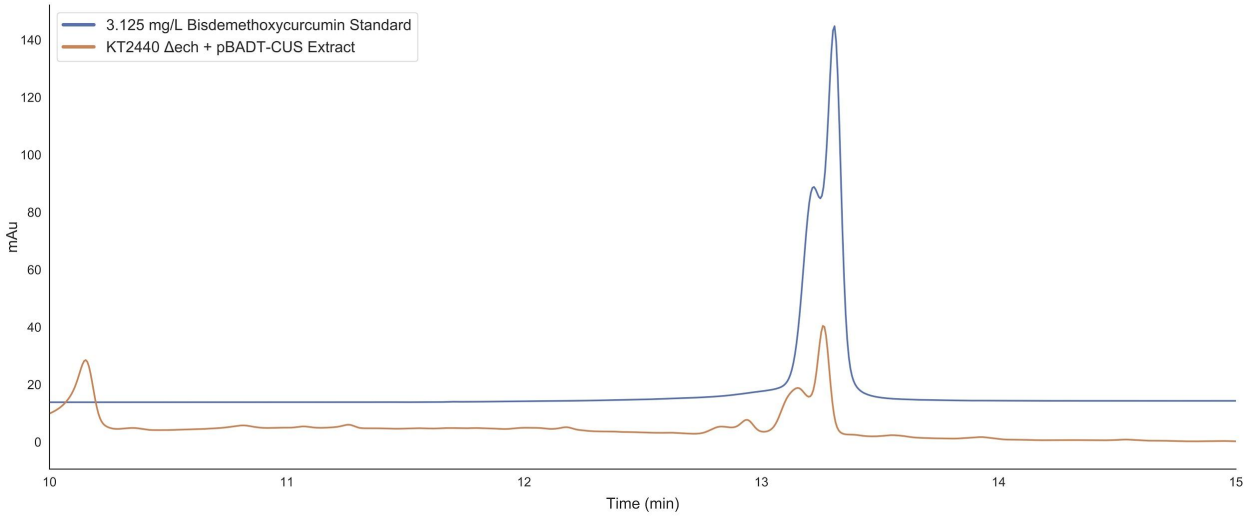

Figure S3: Standard curve of bisdemethoxycurcumin. Absorbance measurements at 425 nm from 50 to 0 mg/L of bisdemethoxycurcumin dissolved in oleyl alcohol.

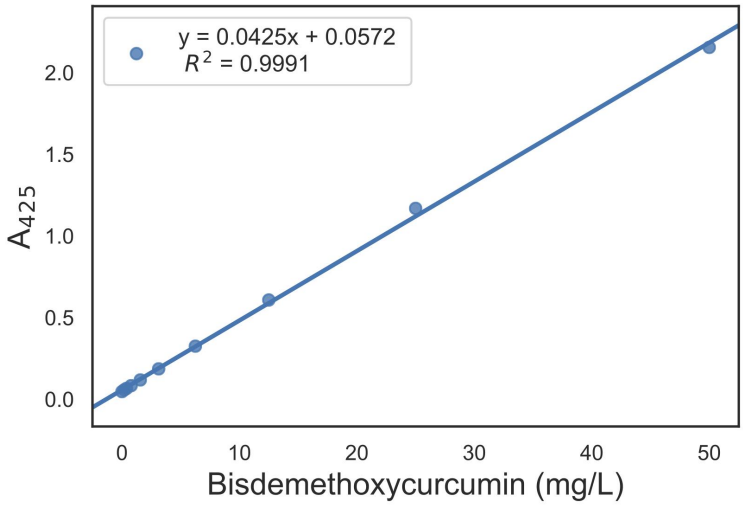

567 **Figure S4:** Production of flaviolin in *P. putida* KT2440 measured with absorbance at 340 nm.
568 Glucose concentrations were varied from 0 mM to 400 mM in MOPS minimal medium.

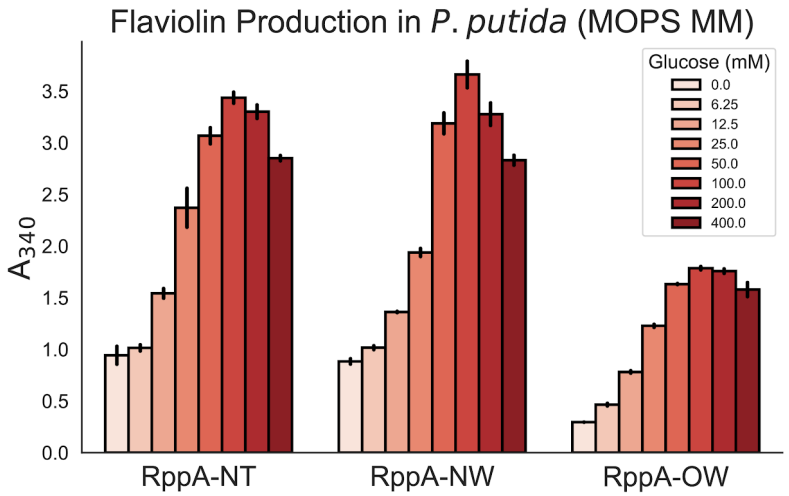

569 **Figure S5:** ^{1}H-NMR spectrum of flaviolin isolated from *P. putida* KT2440 expressing *rppA*-NT
570 from the plasmid pBADT-*rppA*-NT. A) ^{1}H-NMR spectrum from flaviolin freshly resuspended in
571 CD_3OD. B) ^{1}H-NMR spectrum from flaviolin resuspended in CD_3OD and incubated at room
572 temperature overnight. The signal at 5.58 (s, 1 H) is absent in the overnight treatment due to
573 proton exchange with CD_3OD (Snyder et al., 2009).

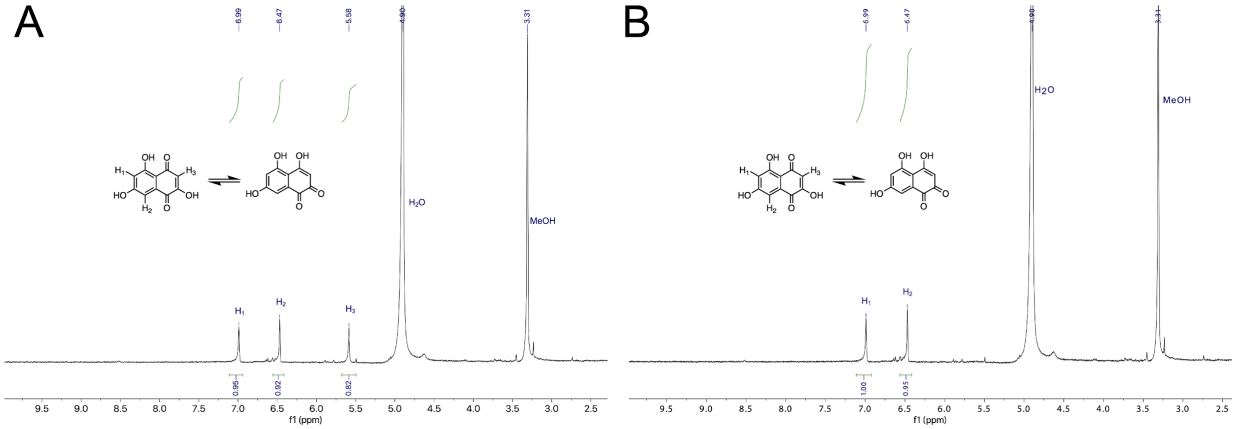

574
575
576
577
578
579
580
581
582
583
584 **Figure S6:** Calculated lagtimes for cultures expressing *fcs* in the presence of 5 mM coumarate.

The *fcs* gene was expressed with 0, 0.05, 0.1, or 0.2% w/v L-arabinose. The lagtimes and their standard deviations are included in the table (right). Lag time is defined here as the amount of time required for the culture to reach OD_{600} = 0.16. Standard deviation was calculated from 3 replicates

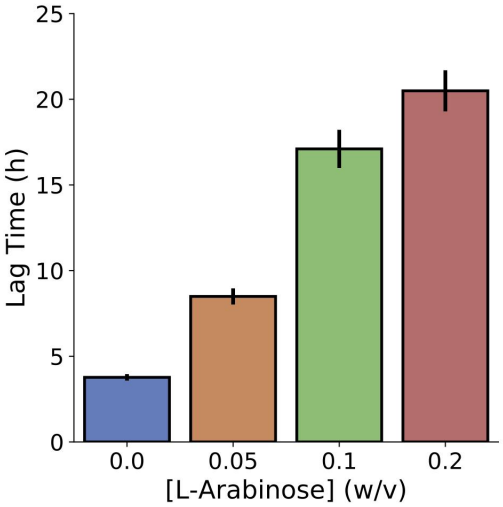

[L-arabinose] (w/v)	Lag Time +/− s.d. (hrs)
0%	3.77 +/− 0.10
0.05%	8.50 +/− 0.44
0.10%	17.10 +/− 1.23
0.20%	20.49 +/− 1.33

Bibliography

625 **Aparicio, T., de Lorenzo, V., Martínez-García, E., 2018. CRISPR/Cas9-Based**
626 **Counterselection Boosts Recombineering Efficiency in Pseudomonas putida.**
627 **Biotechnol. J. 13, e1700161. doi:10.1002/biot.201700161**
628 **Aparicio, T., de Lorenzo, V., Martínez-García, E., 2019. CRISPR/Cas9-enhanced ssDNA**
629 **recombineering for Pseudomonas putida. Microb. Biotechnol. 12, 1076–1089.**
630 **doi:10.1111/1751-7915.13453**
631 **Bi, C., Su, P., Müller, J., Yeh, Y.-C., Chhabra, S.R., Beller, H.R., Singer, S.W., Hillson,**
632 **N.J., 2013. Development of a broad-host synthetic biology toolbox for Ralstonia**
633 **eutropha and its application to engineering hydrocarbon biofuel production. Microb.**
634 **Cell Fact. 12, 107. doi:10.1186/1475-2859-12-107**
635 **Cambray, G., Guimaraes, J.C., Arkin, A.P., 2018. Evaluation of 244,000 synthetic**
636 **sequences reveals design principles to optimize translation in Escherichia coli. Nat.**
637 **Biotechnol. 36, 1005–1015. doi:10.1038/nbt.4238**
638 **Chen, J., Densmore, D., Ham, T.S., Keasling, J.D., Hillson, N.J., 2012. DeviceEditor visual**
639 **biological CAD canvas. J. Biol. Eng. 6, 1. doi:10.1186/1754-1611-6-1**
640 **Chen, Y., Vu, J., Thompson, M.G., Sharpless, W.A., Chan, L.J.G., Gin, J.W., Keasling,**
641 **J.D., Adams, P.D., Petzold, C.J., 2019. A rapid methods development workflow for**
642 **high-throughput quantitative proteomic applications. PLoS ONE 14, e0211582.**
643 **doi:10.1371/journal.pone.0211582**
644 **Cook, T.B., Rand, J.M., Nurani, W., Courtney, D.K., Liu, S.A., Pfleger, B.F., 2018. Genetic**
645 **tools for reliable gene expression and recombineering in Pseudomonas putida. J. Ind.**
646 **Microbiol. Biotechnol. 45, 517–527. doi:10.1007/s10295-017-2001-5**
647 **Engler, C., Kandzia, R., Marillonnet, S., 2008. A one pot, one step, precision cloning**
648 **method with high throughput capability. PLoS ONE 3, e3647.**
649 **doi:10.1371/journal.pone.0003647**
650 **Fang, Z., Jones, J.A., Zhou, J., Koffas, M.A.G., 2018. Engineering Escherichia coli Co-**
651 **Cultures for Production of Curcuminoids From Glucose. Biotechnol. J. 13, e1700576.**
652 **doi:10.1002/biot.201700576**
653 **Gibson, D.G., Young, L., Chuang, R.-Y., Venter, J.C., Hutchison, C.A., Smith, H.O., 2009.**
654 **Enzymatic assembly of DNA molecules up to several hundred kilobases. Nat. Methods**
655 **6, 343–345. doi:10.1038/nmeth.1318**
656 **Grant, S.G., Jessee, J., Bloom, F.R., Hanahan, D., 1990. Differential plasmid rescue from**
657 **transgenic mouse DNAs into Escherichia coli methylation-restriction mutants. Proc**
658 **Natl Acad Sci USA 87, 4645–4649. doi:10.1073/pnas.87.12.4645**
659 **Gross, F., Luniak, N., Perlova, O., Gaitatzis, N., Jenke-Kodama, H., Gerth, K., Gottschalk,**
660 **D., Dittmann, E., Müller, R., 2006. Bacterial type III polyketide synthases:**
661 **phylogenetic analysis and potential for the production of novel secondary metabolites**
662 **by heterologous expression in pseudomonads. Arch. Microbiol. 185, 28–38.**
663 **doi:10.1007/s00203-005-0059-3**
664 **Guarnieri, M.T., Ann Franden, M., Johnson, C.W., Beckham, G.T., 2017. Conversion and**

665 assimilation of furfural and 5-(hydroxymethyl)furfural by Pseudomonas putida
666 KT2440. Metab. Eng. Commun. 4, 22–28. doi:10.1016/j.meteno.2017.02.001
667 Ham, T.S., Dmytriv, Z., Plahar, H., Chen, J., Hillson, N.J., Keasling, J.D., 2012. Design,
668 implementation and practice of JBEI-ICE: an open source biological part registry
669 platform and tools. Nucleic Acids Res. 40, e141. doi:10.1093/nar/gks531
670 Heller, W., Hahlbrock, K., 1980. Highly purified "flavanone synthase" from parsley
671 catalyzes the formation of naringenin chalcone. Arch. Biochem. Biophys. 200, 617–619.
672 doi:10.1016/0003-9861(80)90395-1
673 Hewlings, S.J., Kalman, D.S., 2017. Curcumin: A review of its' effects on human health.
674 Foods 6. doi:10.3390/foods6100092
675 Hillson, N.J., Rosengarten, R.D., Keasling, J.D., 2012. j5 DNA assembly design automation
676 software. ACS Synth. Biol. 1, 14–21. doi:10.1021/sb2000116
677 Hori, Y., Nakaki, K., Sato, M., Mizukami, S., Kikuchi, K., 2012. Development of protein-
678 labeling probes with a redesigned fluorogenic switch based on intramolecular
679 association for no-wash live-cell imaging. Angew Chem Int Ed Engl 51, 5611–5614.
680 doi:10.1002/anie.201200867
681 Izumikawa, M., Shipley, P.R., Hopke, J.N., O'Hare, T., Xiang, L., Noel, J.P., Moore, B.S.,
682 2003. Expression and characterization of the type III polyketide synthase 1,3,6,8-
683 tetrahydroxynaphthalene synthase from Streptomyces coelicolor A3(2). J. Ind.
684 Microbiol. Biotechnol. 30, 510–515. doi:10.1007/s10295-003-0075-8
685 Javeri, I., Chand, N., 2016. Curcumin, in: Nutraceuticals. Elsevier, pp. 435–445.
686 doi:10.1016/B978-0-12-802147-7.00031-0
687 Jiménez, J.I., Miñambres, B., García, J.L., Díaz, E., 2002. Genomic analysis of the aromatic
688 catabolic pathways from Pseudomonas putida KT2440. Environ. Microbiol. 4, 824–
689 841. doi:10.1046/j.1462-2920.2002.00370.x
690 Jiménez, J.I., Pérez-Pantoja, D., Chavarría, M., Díaz, E., de Lorenzo, V., 2014. A second
691 chromosomal copy of the catA gene endows Pseudomonas putida mt-2 with an
692 enzymatic safety valve for excess of catechol. Environ. Microbiol. 16, 1767–1778.
693 doi:10.1111/1462-2920.12361
694 Jönsson, L.J., Alriksson, B., Nilvebrant, N.-O., 2013. Bioconversion of lignocellulose:
695 inhibitors and detoxification. Biotechnol. Biofuels 6, 16. doi:10.1186/1754-6834-6-16
696 Kanehisa, M., 2019. Toward understanding the origin and evolution of cellular organisms.
697 Protein Sci. 28, 1947–1951. doi:10.1002/pro.3715
698 Kanehisa, M., Goto, S., 2000. KEGG: kyoto encyclopedia of genes and genomes. Nucleic
699 Acids Res. 28, 27–30. doi:10.1093/nar/28.1.27
700 Kanehisa, M., Sato, Y., Furumichi, M., Morishima, K., Tanabe, M., 2019. New approach
701 for understanding genome variations in KEGG. Nucleic Acids Res. 47, D590–D595.
702 doi:10.1093/nar/gky962
703 Katsuyama, Y., Funa, N., Miyahisa, I., Horinouchi, S., 2007a. Synthesis of unnatural
704 flavonoids and stilbenes by exploiting the plant biosynthetic pathway in Escherichia

705 coli. Chem. Biol. 14, 613–621. doi:10.1016/j.chembiol.2007.05.004
706 Katsuyama, Y., Matsuzawa, M., Funa, N., Horinouchi, S., 2007b. In vitro synthesis of
707 curcuminoids by type III polyketide synthase from Oryza sativa. J. Biol. Chem. 282,
708 37702–37709. doi:10.1074/jbc.M707569200
709 Katsuyama, Y., Matsuzawa, M., Funa, N., Horinouchi, S., 2008. Production of
710 curcuminoids by Escherichia coli carrying an artificial biosynthesis pathway.
711 Microbiology (Reading, Engl) 154, 2620–2628. doi:10.1099/mic.0.2008/018721-0
712 LaBauve, A.E., Wargo, M.J., 2012. Growth and laboratory maintenance of Pseudomonas
713 aeruginosa. Curr. Protoc. Microbiol. Chapter 6, Unit 6E.1.
714 doi:10.1002/9780471729259.mc06e01s25
715 Lawther, J.M., Sun, R., 1996. The fractional characterisation of polysaccharides and lignin
716 components in alkaline treated and atmospheric refined wheat straw. Industrial Crops
717 and Products 5, 87–95. doi:10.1016/0926-6690(96)00002-7
718 Linger, J.G., Vardon, D.R., Guarnieri, M.T., Karp, E.M., Hunsinger, G.B., Franden, M.A.,
719 Johnson, C.W., Chupka, G., Strathmann, T.J., Pienkos, P.T., Beckham, G.T., 2014.
720 Lignin valorization through integrated biological funneling and chemical catalysis.
721 Proc Natl Acad Sci USA 111, 12013–12018. doi:10.1073/pnas.1410657111
722 Martínez-García, E., de Lorenzo, V., 2011. Engineering multiple genomic deletions in
723 Gram-negative bacteria: analysis of the multi-resistant antibiotic profile of
724 Pseudomonas putida KT2440. Environ. Microbiol. 13, 2702–2716. doi:10.1111/j.1462-
725 2920.2011.02538.x
726 Mills, T.Y., Sandoval, N.R., Gill, R.T., 2009. Cellulosic hydrolysate toxicity and tolerance
727 mechanisms in Escherichia coli. Biotechnol. Biofuels 2, 26. doi:10.1186/1754-6834-2-26
728 Nijkamp, K., van Luijk, N., de Bont, J.A.M., Wery, J., 2005. The solvent-tolerant
729 Pseudomonas putida S12 as host for the production of cinnamic acid from glucose.
730 Appl. Microbiol. Biotechnol. 69, 170–177. doi:10.1007/s00253-005-1973-7
731 Nijkamp, K., Westerhof, R.G.M., Ballerstedt, H., de Bont, J.A.M., Wery, J., 2007.
732 Optimization of the solvent-tolerant Pseudomonas putida S12 as host for the
733 production of p-coumarate from glucose. Appl. Microbiol. Biotechnol. 74, 617–624.
734 doi:10.1007/s00253-006-0703-0
735 Nozaki, M., Kagamiyama, H., Hayaishi, O., 1963. Crystallization and some properties of
736 metapyrocatechase. Biochem. Biophys. Res. Commun. 11, 65–69. doi:10.1016/0006-
737 291X(63)90029-9
738 Overhage, J., Priefert, H., Rabenhorst, J., Steinbüchel, A., 1999. Biotransformation of
739 eugenol to vanillin by a mutant of Pseudomonas sp. strain HR199 constructed by
740 disruption of the vanillin dehydrogenase (vdh) gene. Appl. Microbiol. Biotechnol. 52,
741 820–828. doi:10.1007/s002530051598
742 Parke, D., Ornston, L.N., 2004. Toxicity caused by hydroxycinnamoyl-coenzyme A
743 thioester accumulation in mutants of Acinetobacter sp. strain ADP1. Appl. Environ.
744 Microbiol. 70, 2974–2983.

745 **Park, M.-R., Chen, Y., Thompson, M., Benites, V.T., Fong, B., Petzold, C.J., Baidoo,**
746 **E.E.K., Gladden, J.M., Adams, P.D., Keasling, J.D., Simmons, B.A., Singer, S.W.,**
747 **2019. The response of *Pseudomonas putida* to a complex lignolysate. BioRxiv.**
748 **doi:10.1101/764399**
749 **Park, S.R., Yoon, J.A., Paik, J.H., Park, J.W., Jung, W.S., Ban, Y.-H., Kim, E.J., Yoo, Y.J.,**
750 **Han, A.R., Yoon, Y.J., 2009. Engineering of plant-specific phenylpropanoids**
751 **biosynthesis in Streptomyces venezuelae. J. Biotechnol. 141, 181–188.**
752 **doi:10.1016/j.jbiotec.2009.03.013**
753 **Plaggenborg, R., Overhage, J., Steinbüchel, A., Priefert, H., 2003. Functional analyses of**
754 **genes involved in the metabolism of ferulic acid in Pseudomonas putida KT2440. Appl.**
755 **Microbiol. Biotechnol. 61, 528–535. doi:10.1007/s00253-003-1260-4**
756 **Price, M.N., Ray, J., Iavarone, A.T., Carlson, H.K., Ryan, E.M., Malmstrom, R.R., Arkin,**
757 **A.P., Deutschbauer, A.M., 2019. Oxidative pathways of deoxyribose and**
758 **deoxyribonate catabolism. mSystems 4. doi:10.1128/mSystems.00297-18**
759 **Price, M.N., Wetmore, K.M., Waters, R.J., Callaghan, M., Ray, J., Liu, H., Kuehl, J.V.,**
760 **Melnyk, R.A., Lamson, J.S., Suh, Y., Carlson, H.K., Esquivel, Z., Sadeeshkumar, H.,**
761 **Chakraborty, R., Zane, G.M., Rubin, B.E., Wall, J.D., Visel, A., Bristow, J., Blow,**
762 **M.J., Deutschbauer, A.M., 2018. Mutant phenotypes for thousands of bacterial genes**
763 **of unknown function. Nature 557, 503–509. doi:10.1038/s41586-018-0124-0**
764 **Priefert, H., Rabenhorst, J., Steinbüchel, A., 2001. Biotechnological production of vanillin.**
765 **Appl. Microbiol. Biotechnol. 56, 296–314. doi:10.1007/s002530100687**
766 **Rand, J.M., Pisithkul, T., Clark, R.L., Thiede, J.M., Mehrer, C.R., Agnew, D.E., Campbell,**
767 **C.E., Markley, A.L., Price, M.N., Ray, J., Wetmore, K.M., Suh, Y., Arkin, A.P.,**
768 **Deutschbauer, A.M., Amador-Noguez, D., Pfleger, B.F., 2017. A metabolic pathway**
769 **for catabolizing levulinic acid in bacteria. Nat. Microbiol. 2, 1624–1634.**
770 **doi:10.1038/s41564-017-0028-z**
771 **Santos, C.N.S., Koffas, M., Stephanopoulos, G., 2011. Optimization of a heterologous**
772 **pathway for the production of flavonoids from glucose. Metab. Eng. 13, 392–400.**
773 **doi:10.1016/j.ymben.2011.02.002**
774 **Schanz, S., Schröder, G., Schröder, J., 1992. Stilbene synthase from Scots pine (*Pinus***
775 ***sylvestris*). FEBS Lett. 313, 71–74. doi:10.1016/0014-5793(92)81187-Q**
776 **Shanks, R.M.Q., Kadouri, D.E., MacEachran, D.P., O'Toole, G.A., 2009. New yeast**
777 **recombineering tools for bacteria. Plasmid 62, 88–97.**
778 **doi:10.1016/j.plasmid.2009.05.002**
779 **Smith, L.R., 1996. Rheosmin ("Raspberry Ketone") and Zingerone, and Their Preparation**
780 **by Crossed Aldol-Catalytic Hydrogenation Sequences. Chem. Educator 1, 1–18.**
781 **doi:10.1007/s00897960034a**
782 **Snyder, S.A., Tang, Z.-Y., Gupta, R., 2009. Enantioselective total synthesis of (-)-**
783 **napyradiomycin A1 via asymmetric chlorination of an isolated olefin. J. Am. Chem.**
784 **Soc. 131, 5744–5745. doi:10.1021/ja9014716**

785 **Soga, O., 1982. Stimulative Production of Flaviolin by *Phoma wasabiae*. Agric. Biol. Chem.**
786 **46, 1061–1063. doi:10.1080/00021369.1982.10865194**
787 **Thompson, Mitchell G., Blake-Hedges, J.M., Cruz-Morales, P., Barajas, J.F., Curran, S.C.,**
788 **Eiben, C.B., Harris, N.C., Benites, V.T., Gin, J.W., Sharpless, W.A., Twigg, F.F.,**
789 **Skyrud, W., Krishna, R.N., Pereira, J.H., Baidoo, E.E.K., Petzold, C.J., Adams, P.D.,**
790 **Arkin, A.P., Deutschbauer, A.M., Keasling, J.D., 2019. Massively Parallel Fitness**
791 **Profiling Reveals Multiple Novel Enzymes in Pseudomonas putida Lysine Metabolism.**
792 **MBio 10. doi:10.1128/mBio.02577-18**
793 **Thompson, Mitchell G, Valencia, L.E., Blake-Hedges, J.M., Cruz-Morales, P., Velasquez,**
794 **A.E., Pearson, A.N., Sermeno, L.N., Sharpless, W.A., Benites, V.T., Chen, Y., Baidoo,**
795 **E.E.K., Petzold, C.J., Deutschbauer, A.M., Keasling, J.D., 2019. Omics-driven**
796 **identification and elimination of valerolactam catabolism in Pseudomonas putida**
797 **KT2440 for increased product titer. Metab. Eng. Commun. 9, e00098.**
798 **doi:10.1016/j.mec.2019.e00098**
799 **Wakimoto, T., Morita, H., Abe, I., 2012. Engineering of plant type III polyketide synthases.**
800 **Meth. Enzymol. 515, 337–358. doi:10.1016/B978-0-12-394290-6.00016-1**
801 **Wang, Y., Horlamus, F., Henkel, M., Kovacic, F., Schläfle, S., Hausmann, R., Wittgens, A.,**
802 **Rosenau, F., 2019. Growth of engineered*Pseudomonas putida* KT2440 on glucose,**
803 **xylose and arabinose: hemicellulose hydrolysates and their major sugars as**
804 **sustainable carbon sources. Glob. Change Biol. Bioenergy. doi:10.1111/gcbb.12590**
805 **Wetmore, K.M., Price, M.N., Waters, R.J., Lamson, J.S., He, J., Hoover, C.A., Blow, M.J.,**
806 **Bristow, J., Butland, G., Arkin, A.P., Deutschbauer, A., 2015. Rapid quantification of**
807 **mutant fitness in diverse bacteria by sequencing randomly bar-coded transposons.**
808 **MBio 6, e00306-15. doi:10.1128/mBio.00306-15**
809 **Wightman, F., Lighty, D.L., 1982. Identification of phenylacetic acid as a natural auxin in**
810 **the shoots of higher plants. Physiol. Plant. 55, 17–24. doi:10.1111/j.1399-**
811 **3054.1982.tb00278.x**
812 **Wirth, N.T., Kozaeva, E., Nikel, P.I., 2019. Accelerated genome engineering of**
813 **Pseudomonas putida by I-SceI-mediated recombination and CRISPR-Cas9**
814 **counterselection. Microb. Biotechnol. doi:10.1111/1751-7915.13396**
815 **Yang, D., Kim, W.J., Yoo, S.M., Choi, J.H., Ha, S.H., Lee, M.H., Lee, S.Y., 2018.**
816 **Repurposing type III polyketide synthase as a malonyl-CoA biosensor for metabolic**
817 **engineering in bacteria. Proc Natl Acad Sci USA 115, 9835–9844.**
818 **doi:10.1073/pnas.1808567115**
819 **Yu, D., Xu, F., Zeng, J., Zhan, J., 2012. Type III polyketide synthases in natural product**
820 **biosynthesis. IUBMB Life 64, 285–295. doi:10.1002/iub.1005**
821 **Zang, Y., Zha, J., Wu, X., Zheng, Z., Ouyang, J., Koffas, M.A.G., 2019. In Vitro**
822 **Naringenin Biosynthesis from p-Coumaric Acid Using Recombinant Enzymes. J.**
823 **Agric. Food Chem. doi:10.1021/acs.jafc.9b00413**